MODHIS:

Multi-Objective Diffraction-limited High-resolution Infrared Spectrograph

Detailed Science Case

TMT.INS.TEC.22.033

October 1, 2024

Submitted by:

University of California, San Diego
University of California, Los Angeles
California Institute of Technology
The MODHIS Science Team

Revision History

Date	Revision No.	Revised By	Description
Feb 2022	0.1	Dimitri Mawet	Initial Draft
03 Aug 2022	1.0	Quinn Konopacky et al.	Release for MODHIS CoDR-1 review
23 Jan 2024	1.1	Quinn Konopacky et al.	Updated with polarimetry science cases for CoDR-2 review

Authors and Contributors

Quinn Konopacky (**Project Scientist**, UC San Diego)
Dimitri Mawet (**Principal Investigator**, Caltech)
Michael Fitzgerald (**Co-Principal Investigator**, UC Los Angeles)
Hiroshi Terada (**Project Manager, TMT**)
Richard Dekany (**Work Package Manager**, Caltech)

MODHIS Science Team Members:
Étienne Artigau (U de Montréal)
Ravinder Banyal (IIA)
Thomas Beatty (U of Arizona)
Chas Beichman (Caltech/JPL)
Björn Benneke (U de Montréal)
Geoff Blake (Caltech)
Adam Burgasser (UC San Diego)
Gabriela Canalizo (UC Riverside)
Guo Chen (Purple Mountain Obs.)
Richard Dekany (Caltech)
Tuan Do (UCLA)
Greg Doppmann (WMKO)
René Doyon (U de Montréal)
Courtney Dressing (UC Berkeley)
Min Fang (Xiamen U.)
Mike Fitzgerald (UCLA)
Tom Greene (NASA Ames)
Greg Herczeg (KIAA Peking)
Lynne Hillenbrand (Caltech)
Andrew Howard (Caltech)
Nem Jovanovic (Caltech)
Stephen Kane (UC Riverside)
Tiffany Kataria (JPL)
Eliza Kempton (U of Maryland)
Heather Knutson (Caltech)
Quinn Konopacky (UC San Diego)
Takayuki Kotani (ABC / NAOJ)
David Lafrenière (U de Montréal)
Chao Liu (NAOC)
Dimitri Mawet (Caltech)
Stan Metchev (Western U.)
Max Millar-Blanchaer (UC Santa Barbara)
Shogo Nishiyama (Miyagi Education U.)
Gajendra Pandey (IIA)
Peter Plavchan (George Mason U)
S.P. Rajaguru (IIA)
Paul Robertson (UC Irvine)
Colette Salyk (Vassar)
Bunei Sato (Tokyo Inst. of Tech.)
Everett Schlawin (U of Arizona)
Sujan Sengupta (IIA)
Thirupathi Sivarani (IIA)
Warren Skidmore (TMT)
Motohide Tamura (NAOJ)
Hiroshi Terada (TMT)
Gautam Vasisht (JPL)
Jason Wang (Northwestern)
Ji Wang (Ohio State)
Hui Zhang (Nanjing U.)

IRIS Technical Members and other contributors:
John Canfield (UCLA)
Eric Chisholm (TMT)
Alexandre Delacroix (Caltech)
Jennifer Dunn (NRC Herzberg Astronomy and Astrophysics)
Lauren Fahey (Caltech)
Mitsuko Roberts (Caltech)
Roger Smith (Caltech)
Ryuji Suzuki (NAOJ)
Gelys Trancho (TMT

TABLE OF CONTENTS

1. Exoplanet Science Cases

Twenty-five years after the discovery of the first planet orbiting a star other than the Sun, it is now clear that extrasolar planets are ubiquitous in the galaxy. Though our understanding of exoplanet demographics has dramatically expanded in recent years, many fundamental questions about their origin and composition remain. For example, we lack a complete understanding of the chemical and physical processes shaping exoplanet atmospheres, including a full description of their clouds, the abundances of specific species,and the role of disequilibrium chemistry (Beatty et al., 2019; Gao et al., 2020; Madhusudhan, 2019). Additionally, outstanding questions remain about the preferred formation pathways of planets across the entire mass range, particularly for massive planets where no single theory can fully explain the entire population (Dodson-Robinson et al., 2009). The next decade presents a truly unique opportunity in the young history of exoplanetary astronomy. For the first time, we have the observational techniques, the theoretical models, and a sufficient number of known exoplanets orbiting nearby stars to spectroscopically characterize a wide diversity of planets – from hot giant planets to temperate Earth-size planets. Spectroscopic observations hold the key to answering these outstanding questions about planet formation and evolution. However, these observations are extremely challenging. Teasing out the small exoplanet signal from the stellar photon shot noise and calibrating systematics require both high sensitivity and spectro-photometric measurement precision.

Current studies have thus far focused on photometric or low-resolution spectroscopic measurements. This research (e.g., HST and Spitzer studies of transiting planets, and adaptive optics photometry and spectroscopy of directly imaged planets) has yielded critical new insights

into the bulk properties of planet atmospheres at both close (e.g., Sing et al., 2016) and wide separations (e.g., Rajan et al., 2017). Indeed, JWST will inherit this mantle, offering a new observing regime for a wide range of exoplanets. However, JWST's maximum R∼3,000 spectral resolution and its 6.5-meter aperture (small relative to TMT), will not be able to explore the full range of exoplanet science that is critical to advancing the field. This is because, at low spectral resolution (R≲5,000), overlapping spectral bands can lead to degeneracies, minor chemical species important to understand the chemical processes often remain masked, and clouds substantially mute broad spectral signatures (**Figure 1** and Kreidberg et al., 2014; Hood et al., 2020; Gandhi et al., 2020). Furthermore, at low spectral resolutions the spectral line position and line shape information necessary to detect and constrain exoplanetary wind are smeared out.

High-resolution spectroscopy (R∼100,000) has recently emerged as a powerful tool for exoplanet studies (e.g., Snellen et al., 2010; Brogi et al., 2012; Birkby et al., 2013; Brogi et al., 2013, 2014; Snellen et al., 2014; Crossfield, 2014; Snellen et al., 2015; Brogi et al., 2016; Birkby et al., 2017; Birkby, 2018; Wang et al., 2021). For the future, it is the necessary complement to current and upcoming low and moderate resolution capabilities (Brogi et al., 2017; Brogi and Line, 2019). High spectral resolution offers the opportunity to distinguish the planet signal from stellar and telluric contamination via the wealth of information contained in the resolved and Doppler-shifted NIR atomic and molecular features in the planet's atmosphere (Figure 1). With an appropriate design, a NIR high-resolution spectrograph on a large, ground-based telescope can study exoplanets via three major methods of exoplanet detection and characterization (transit spectroscopy, direct imaging, and radial velocity). This is the fundamental driver behind MODHIS's design, which will offer a paradigm shift in observational studies of exoplanets.

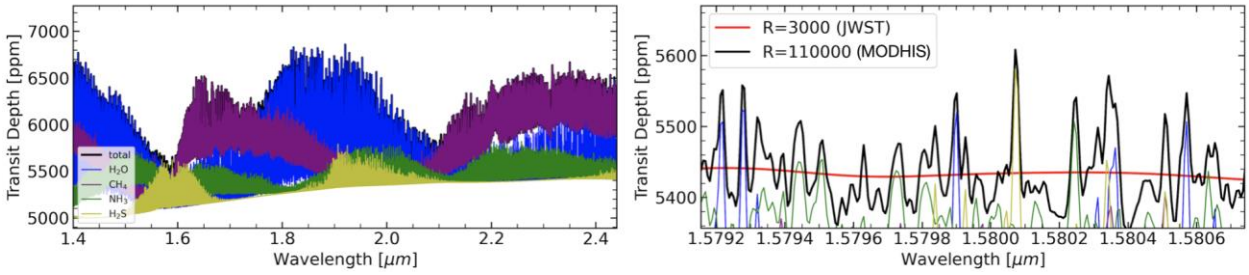

Figure 1: *The two panels show fiducial model transmission spectra of a typical 500 K sub-Neptune at MODHIS's native spectral resolution, with the colors highlighting the contribution from individual molecules. The HK (red) wavelength domain of MODHIS is illustrated in the left panel and a zoom in of 1.579–1.582 μm is shown in the right panel. All major carbon-, oxygen-, nitrogen-, and sulfur-bearing molecules show a large number of prominent features in the wavelength range covered by MODHIS (left panel). CO and CO_2 are also spectrally-active in this range, but not shown because the displayed 500 K sub-Neptune atmosphere is not expected to contain much CO and CO_2. The right panel highlights the benefits of high-resolution spectroscopy for exoplanet characterization. At the comparatively coarse resolution of JWST-NIRSpec (red curve), the spectral lines of H_2O (blue), NH_3 (green), and H_2S (yellow) are all blurred together masking the contributions from minor molecules. MODHIS's high resolving power (black curve) will reveal their individual contributions and relative abundances using the cross-correlation technique.*

MODHIS's distinctive combination of sensitivity (thanks to TMT's 30-meter collecting aperture), simultaneous spectral coverage at R>100,000 (y, J, H and K bands), internal instrument stability (<0.5 m/s) and unique high-contrast operation at TMT's diffraction limit offers new opportunities to shed light on exoplanet atmospheric chemistry and dynamics, as well as formation mechanisms. For certain classes of planets, i.e. those orbiting very cool or active stars, or stars in binary systems, MODHIS also offers the ability to obtain masses and additional orbital information.

1.1. Atmospheres of Close-in Exoplanets

Heated by their host stars, close-in exoplanets (orbital separations of <0.01 AU) have prominent observable atmospheric features, which make them ideal targets for characterization. Indeed, some of the most detailed data we have on planetary atmospheres outside the Solar System comes from hot Jupiters (Stevenson et al. 2014). This will continue to be the case for at least the next decade.

The general goal of these types of atmospheric observations is to measure both the bulk abundances of the planetary atmospheres, as well as specific elemental abundance ratios (usually C/H, O/H, and N/H). These two types of measurements allow us to test test theories of planet formation via trends in bulk metallicity (e.g., Mordasini et al. 2016) and to directly probe the planet formation pathways via elemental abundance measurements (e.g., Madhusudhan et al. 2017). Atmospheric observations of close-in exoplanets can also identify potentially habitable, warm and temperate, atmospheres on super-Earths orbiting lower-mass M-dwarfs (Madhusudhan et al. 2021).

One method to measure the atmospheres of close-in exoplanets is using transit and eclipse spectroscopy of transiting planets. MODHIS transit observations of close-in exoplanets provides a unique tool to explore the compositional diversity of planets and their atmospheres, by determining the bulk elemental compositions of giant planet envelopes. Transit spectroscopy also explores the nature of clouds and hazes on these planets, and can be used to search for atmospheres of sub-Neptunes and terrestrial exoplanets — plausibly even with temperate conditions.

MODHIS will also be able to conduct high-resolution spectroscopic observations of close-in exoplanets to measure atmospheric abundances and temperature structure, and can do so for both transiting and non-transiting exoplanets. Currently, exoplanet atmospheric characterization using these types of high-resolution spectroscopy observations cross-correlate against the entire planetary spectrum (e.g., Snellen et al. 2010), which yield good overall molecular abundances. Excitingly, the large aperture of TMT and the high sensitivity of MODHIS mean that we will be able to conduct this same observations on a line-by-line basis, thereby constructing a real high-resolution spectrum of the planetary atmosphere. We can then use the relative strengths of these individual lines in a molecular band to directly constrain the temperature structure of a planets' atmosphere, along with measuring specific elemental abundances.

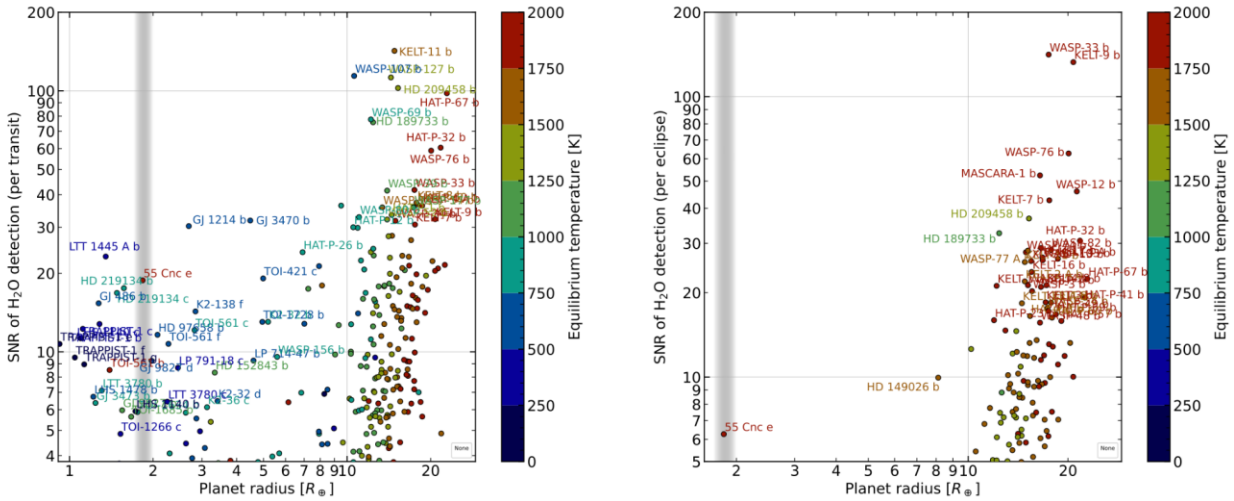

Figure 2: *Selected targets for transit observations (left) and secondary eclipse observations (right). All labeled planets can be observed with MODHIS, representing the most favorable targets among all known transiting planets with declinations observable from Maunakea (circles). The signal-to-noise ratio of water detections in a hydrogen-dominated atmosphere is indicated versus the planet radius, with the color indicating the equilibrium temperature. SNRs are calibrated using true injection-recovery tests using cross-correlation analyses on sequences of realistically simulated TMT-MODHIS exposures that included tellurics and instrumental noise. Planets below 5 R⊕ will be observed 3 to 8 times over multiple observing cycles to build up SNR to probe for high mean molecular mass (e.g. GJ 9827c, 55 Cnc e) and highly hazy/cloudy atmospheres (e.g. GJ 1214b). The green vertical line indicates the position of the radius valley in the small planet occurrence rates believed to separate rocky planets and sub-Neptunes (Fulton et al. 2017).*

For hot Jupiters and warm Neptunes, high-resolution transmission spectroscopy has been used to detect molecular gas (Snellen et al., 2010; Birkby et al., 2013; de Kok et al., 2014) and to study day to night-side wind velocity (Snellen et al., 2010; Brogi et al., 2016; Seidel et al., 2020) and night-side condensation of volatile species such as iron Ehrenreich et al. (2020), providing an ultimate test for 3D exoplanet global circulation models (Miller-Ricci Kempton and Rauscher, 2012; Zhang et al., 2017; Harada et al., 2019; Flowers et al., 2019; Beltz et al., 2021). These results demonstrate the unique view that transit spectroscopy provides us into the menagerie of planetary atmospheres and their clouds.

By the time MODHIS begins its observations, the Transiting Exoplanet Survey Satellite (TESS) and PLATO will have already explored the entire sky to identify the most favorable exoplanet targets, and many of these planets will have very precise, but low resolution (100<R<1000), atmospheric spectra from JWST.

MODHIS will be a game-changer in this scientific environment. The instrument will particularly excel for cloudy and hazy atmospheres (e.g., GJ 1214b) because the narrow cores of molecular lines observable at high resolution (R>80,000) form above the clouds (Hood et al. 2020; Gandhi et al. 2020), unlike the broad molecular bands observable at low and medium resolution with JWST (Figure 2) which are muted by the presence of clouds (Kreidberg et al. 2014). In addition, the

narrow planetary molecular lines shift in velocity during the transit, enabling an unambiguous distinction from any H2O or CO stellar or telluric lines (Rackham et al. 2018).

1.2. Chemodynamics of Directly Imaged Exoplanets

The question "How do planets form?" is best answered by characterizing them near the epoch of their formation. This can be achieved on Solar System scales with MODHIS (1-100 AU), which combines high angular resolution, high-contrast, and high-resolution spectroscopy (Snellen et al., 2014, 2015; Hoeijmakers et al., 2018; Bowler et al., 2019), a technique also known as High Dispersion Coronagraphy (HDC, Wang et al., 2017; Mawet et al., 2017, Figure 3). The AO system separates the light from the star and the companion, whose signals are then individually fed to the spectrograph via SMFs for further spectral differentiation. Furthermore, using HDC as a pathway to habitable worlds with the ELTs is one of the four key capabilities laid out by Astro2020 (National Academies of Sciences, Engineering, and Medicine, 2021, see their §1.1.1).

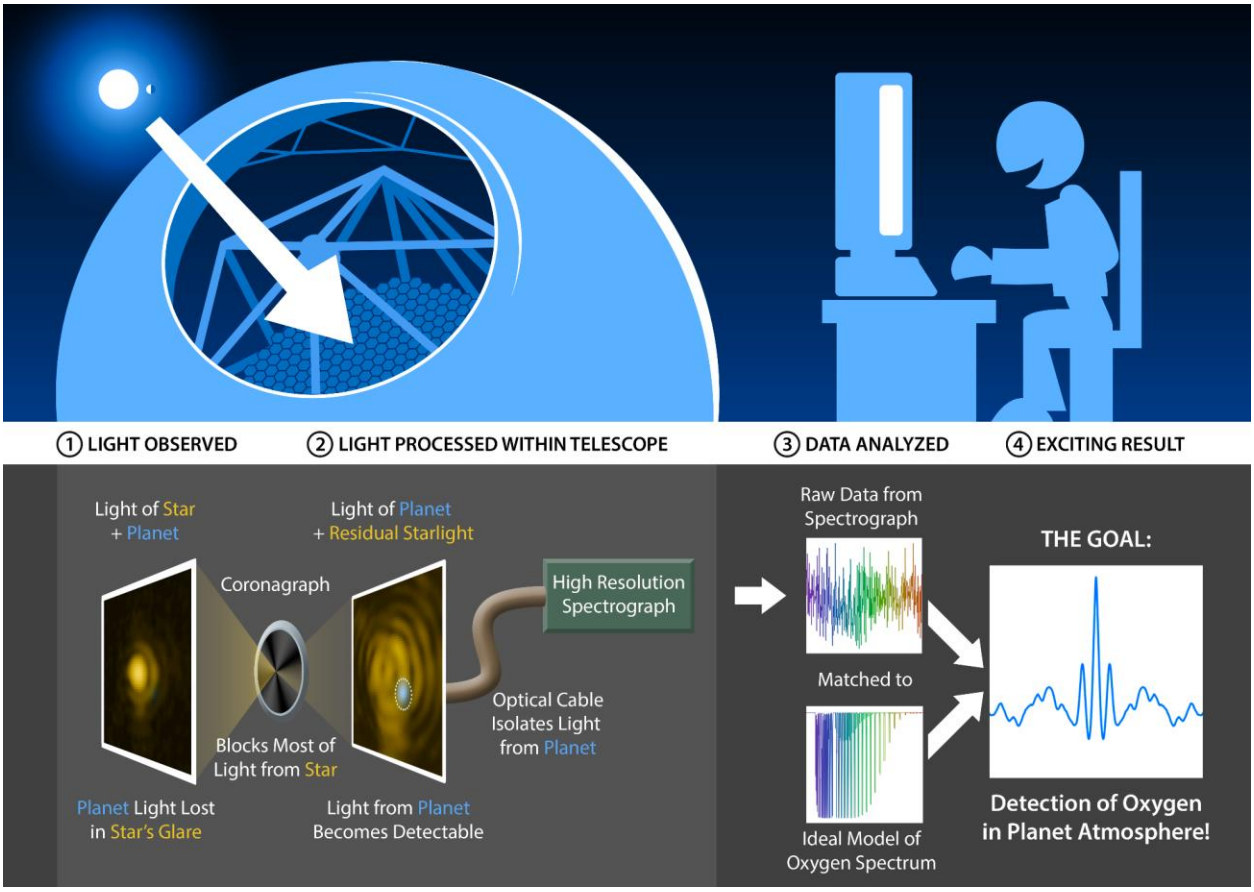

Figure 3: Working principles High-Dispersion Coronagraphy, a core functionality of TMT-MODHIS.

1.2.1. Giant Planets

MODHIS will be able to survey directly imaged giant planets beyond 0.1 au (Figure 4), enabling the spectroscopic characterization of ~100 giant planets. This range of separations includes the peak in giant exoplanet occurrence rates at ~2.5 AU as measured by RV surveys (Fernandes et al., 2019; Rosenthal et al., 2021), allowing us to study the most typical giant planets and place our

own Jupiter into context. By studying the shapes of spectral lines at high spectral resolution, MODHIS will be able to measure the compositions, spins, and orbits of typical giant planets at a population level. Models of core accretion and late-stage planetesimal accretion predict gradients in the metallicities and elemental abundance ratios of giant planets as a function of mass and semi-major axis (Cridland et al. 2020). Current leading theories that magnetic breaking in the protoplanetary disk sets the final spin rates of giant planets predicts gradients in spin speeds as a function of mass (Batygin, 2018). Measuring the eccentricity distribution of typical giant planets will inform us whether giant planets create dynamically quiescent planetary systems like our own. MODHIS will empirically find the trends that exist in these planet properties that will serve as some of the only constraints to highly complex planet formation models

Additionally, MODHIS will be able to characterize planets at various key stages in their formation and evolution: 1) newborn (1 Myr) protoplanets residing in nearby (~140 pc) star-forming regions to witness planet formation in action; 2) adolescent (~30 Myr) planets that recently finished forming and are still radiating away the signatures of their formation process; 3) mature (> 1 Gyr) planets. MODHIS will be able to study the time evolution of planetary characteristics. Planetary orbits evolve through gravitational interactions and the amount orbits change informs us how dynamically hot planetary systems are. Atmospheric composition changes due to accretion of solids and gases from the circumstellar disk. If magnetic breaking with the protoplanetary disk is indeed responsible for setting planetary spin rates, protoplanets likely have a different spin distribution than older planets for which angular momentum is conserved.

While the majority of these planets are yet to be discovered, MODHIS is capable of either discovering them or following up indirectly discovered planets. The Gaia astrometric mission will uncover thousands of new giant exoplanets (Perryman et al., 2014) regardless of their age. Radial velocity has discovered many mature planets beyond 1 au (e.g., Rosenthal et al. 2021), and precise infrared spectrographs like MODHIS itself will find adolescent giant planets. MODHIS will focus on follow-up characterization of these indirectly discovered planets. MODHIS will also have a discovery mode: the vortex fiber nuller (VFN; Ruane et al. 2018, Echeverri et al. 2019). VFN combines nulling interferometry with high resolution spectroscopy and enables the discovery and characterization of exoplanets at any position ~1 λ/D away from the star.

A unique addition capability of MODHIS is the ability to perform resolved spectroscopy of previously unresolved worlds. Due to the angular resolution of TMT, planets around nearby (~10 pc) stars residing between 0.01 and 1 au can be spatially resolved for the first time (Fig. 4). These planets are bright due to being close to their host stars, but are far enough away that MODHIS can suppress the light of their host stars, unlike current thermal emission studies of close-in planets with current ground-based observatories or with JWST. This allows for a unique sensitivity window for MODHIS to study planets at the boundary of Neptune and Saturn (0.l Jupiter masses).

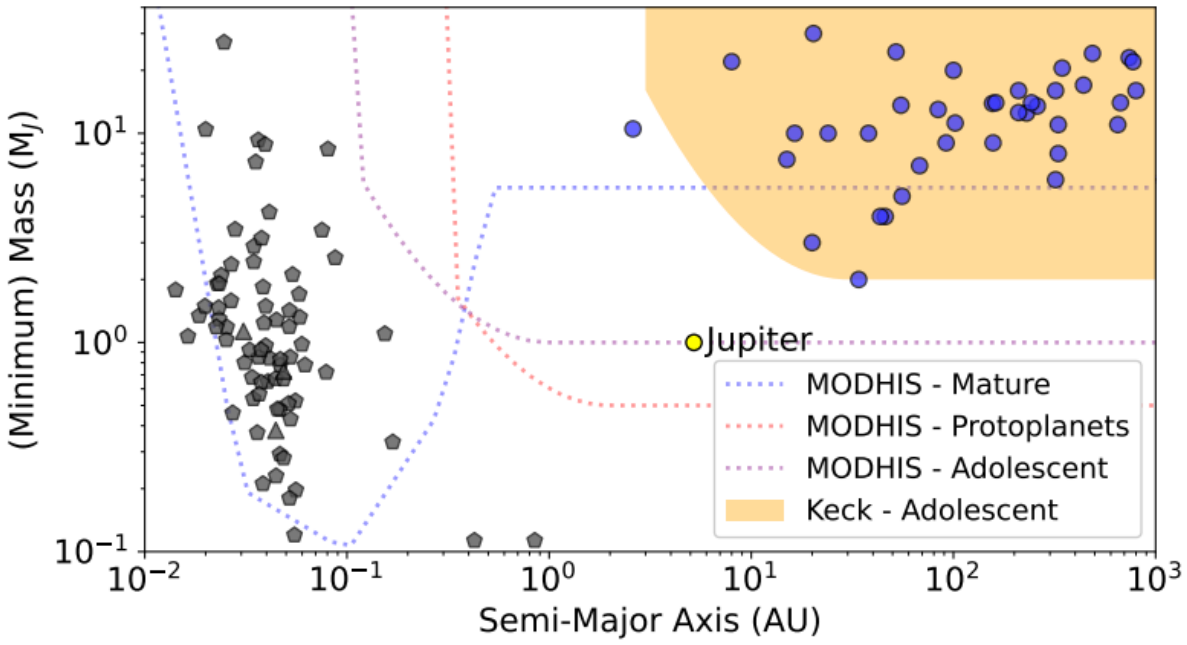

Figure 4: *Sensitivity of MODHIS for direct spectroscopy of exoplanets for three different classes of planets: protoplanets (1 Myr old) residing in the closest (140 pc) star-forming regions, adolescent (40 Myr) planets residing in nearby (30 pc) young moving groups, and mature (1 Gyr) planets residing in the Solar neighborhood (10 pc). Sensitivity limits were computed with the MODHIS exposure time calculator. For protoplanets and adolescent planets, the planets are dominated by the glow from their heat of formation. For mature planets close-in (< 1 au), thermal heating and reflected light become dominant contributors, allowing for increased sensitivity close-in.*

1.2.2. Terrestrial Worlds

One of the top goals of exoplanet science is finding other habitable worlds. By combining the high angular resolution and high spectral resolution capabilities together, MODHIS offers us the first attempt to directly measure the spectra of exoplanets residing in the habitable zone around other nearby stars. In particular, MODHIS operating behind the NFIRAOS AO system is capable of reaching the necessary starlight suppression to detect and characterize Proxima b, the closest terrestrial planet that resides in the habitable zone of its host star (Wang et al. 2017). There are also a handful of other nearby low-mass stars that MODHIS is capable of detecting habitable zone exo-Earths around (Ruane et al. 2019). For these stars, there is incomplete knowledge whether they harbor terrestrial planets in their habitable zones, but upcoming precise infrared spectrographs like MODHIS would be capable of detecting these planets indirectly before performing any direct spectroscopy observations. While it is only a handful of systems and the habitability of planets around low-mass stars is still uncertain, this would likely be our first attempt to perform direct spectroscopy of an exo-Earth candidate, and should not be missed.

1.3. Exoplanet Masses, Orbits, and Discovery with NIR PRV

MODHIS uniquely offers extreme sensitivity for Precision Radial Velocity measurements (PRV) for cool stars and close binaries requiring high angular resolution. With its instrumental stability

requirement of <0.3 m/s MODHIS will be able to detect and characterize rocky Earths and super Earths orbiting in the Habitable Zones (HZ) of late type M stars as shown Fig. 5 (in units of Earth masses) and (Fig. 6 in m/s) for the representative K band. The PRV precision resulting from combining all four wavelength bands will be roughly a factor of two better than that of an individual band, with the exact degree of improvement depending on stellar temperature. An aspect of combining the wavelengths not captured in these figures is the benefit of such a wide wavelength grasp in reducing the effects of stellar variability (Plavchan et al 2020).

While the practical PRV sensitivity limit will likely be set by the effects of telluric absorption, ∼1 m/s in a single measurement after post-processing (see below), MODHIS will achieve this limiting sensitivity for stars otherwise inaccessible due to their faintness. There are over 50 M dwarfs later than M5 (G-H>4 mag, Pecaut & Mamajek (2013)) within 25 pc with H <12 mag which would be easily within the grasp of MODHIS to detect HZ Earth analogs. While it is unlikely that MODHIS will be used to survey large numbers of stars due to the tens of individual measurements required per star, some of the faintest stars not examined by on-going surveys could be studied with TMT.

MODHIS will, however, be extremely well suited for detailed characterization of systems found by surveys on smaller telescopes. MODHIS will be able to determine RV masses for small, temperate, new planets orbiting cool stars such as Trappist-1 which will be discovered by TESS or other surveys. There are currently only 26 confirmed transiting planets orbiting M dwarfs with $R < 2R_{\oplus}$ with RV masses and none are located in the HZs of their host stars. There are only two HZ systems orbiting M stars with TTV-determined masses (Trappist-1 and Kepler 138) with many Kepler, K2 or TESS candidates with planet equilibrium temperatures $\leq$300 K and $R \leq 2R_{\oplus}$ awaiting confirmation and characterization. TESS's extended mission will continue to add new objects to this important population. In addition to enabling the follow up of these systems, there are a number of specific NIR PRV science cases uniquely enabled by MODHIS.

1.3.1. Orbital Obliquity of Planets Orbiting Young and/or Cool Stars

Orbital obliquity, the angle between the stellar spin axis and a planet's angular momentum vector, places crucial constraints on planet formation and migration mechanisms since large mutual inclinations can be highly disruptive in multiple systems (Winn and Fabrycky, 2015; Ormel et al., 2017). The obliquity is measured via the Rossiter- McLaughlin (RM) effect which changes the RV signature during a transit (Triaud, 2018). HISPEC will also be able to determine the obliquity via the "Doppler-shadow" analysis that directly detects the profile variation of the cross-correlation function of the observed spectra (Gaidos et al., 2022). These time series observations last only a few hours and require the excellent instantaneous sensitivity provided by an instrument on a 30 m telescope. With each observation lasting only a few hours, MODHIS could measure obliquities of ~50 planets ranging in size from super-Earths and sub-Neptunes orbiting late M (Teff<4000 K) stars. Only one system cooler than 4000 K, GJ436, currently has a published obliquity (Bourrier et al., 2018). MODHIS will also provide obliquity determinations for planets orbiting young stars. Gaidos et al. (2022) recently used Subaru's IRD spectrometer to determine that V1298 Tau b is in a $\lambda \sim 15^{\circ}$ prograde orbit, suggesting that the four planets in the system formed in a flat co-planar disk. The statistics of the population of young and mature stars will provide important constraints to theories of planet formation and evolution

1.3.2. Young Planets

The early evolution of young, still-contracting planets is poorly understood (Fortney et al., 2008; Spiegel and Burrows, 2013). K2 has identified planets transiting young host stars in Young Moving Groups (∼50–90 Myr; David et al. (2018)) and open clusters (∼600–800 Myr; Mann et al. (2017); Ciardi et al. (2018)) and TESS is discovering many more, e.g. AU Mic b (Plavchan et al., 2020). Among these are hot Jupiters with large predicted Doppler semi-amplitudes of ∼10–100 m/s. With the demonstrated 2–4× reduction in the effects of stellar activity relative to visible wavelengths (e.g. Johns-Krull et al., 2016; Carleo et al., 2018; Klein et al., 2020), MODHIS will determine the masses of young transiting planets and address the initial density of exoplanets. Recent PRV results for the 20 Myr old star V1298 Tau suggest a surprisingly high initial densities for two of its Jupiter-sized planets (Mascareno et al 2021) compared with theoretical expectations (Mordasini et al 2012abc; Fortney et al 2007). While additional observations have called this result into question, the fact remains that this is an area of intense observational and theoretical interest which will require extensive observations for its resolution. The accurate determination of the masses and radii of young planets will be critical to understanding the mechanism(s) responsible for the "Fulton Gap" in the Planet Radius-Orbital Period plane (David et al., 2021; Pascucci et al., 2019). Understanding whether or not the population of dense super-Earths found in transit surveys initially formed as rocky bodies or started out as larger, gas rich bodies but lost their H2 rich atmospheres to end up as rocky cores pertains directly to the occurrence rate of Habitable Zone Earth-analogs which are the targets for future direct imaging space missions (Pascucci et al 2019).

1.3.3. Exomoons

Several exomoon candidates have been proposed to date (e.g. Kipping et al. 2022, Lazzoni et al. 2020), but none have been confirmed. As part of the formation process of exoplanets, exomoons are an important missing piece to better understand planetary systems and can strongly influence the atmospheres of giant exoplanets (e.g. interaction between Io and Jupiter). Icy moons around gas giants are also interesting targets as they could develop life (Reynolds et al. 1983).

Similarly to the detection of planets with radial velocity (RV) surveys of stars, measuring the radial velocity of planets and brown-dwarfs is a promising technique to search for binary planets and exomoons (Vanderburg et al. 2018). The mass ratio of moons relative to their planet is expected to be around 10^{-4} (Canup & Ward 2006), which is consistent with Ganymede around Jupiter for example. This small mass ratio could explain the lack of current detections.

Using RV measurements from a R=4,000 spectrograph at Keck and the first planetary RV time series (Ruffio et al. 2021), Vanderburg & Rodriguez (2021) derived the first exomoon mass upper limits with this technique around the HR 8799 planets. They ruled out Jupiter-mass moons orbiting the 7 Jupiter masses planet HR 8799 c in periods shorter than 1 day.

We predict an RV precision of 5 m/s in 10-minute exposures for the same planet with TMT/MODHIS thanks to the higher spectral resolution (R=100,000) and bigger telescope.

Batygin & Morbidelli (2020) suggests that the moon mass roughly scales with the planet mass to the 3/2 power, making larger planets harbor comparatively larger moons. Therefore scaling the Galilean moons to the mass of HR 8799 c, they would be detectable with TMT/MODHIS in only a few nights of observations. Additionally, other moon formation mechanisms are likely to generate larger objects such as collision or capture, which would be more easily detectable.

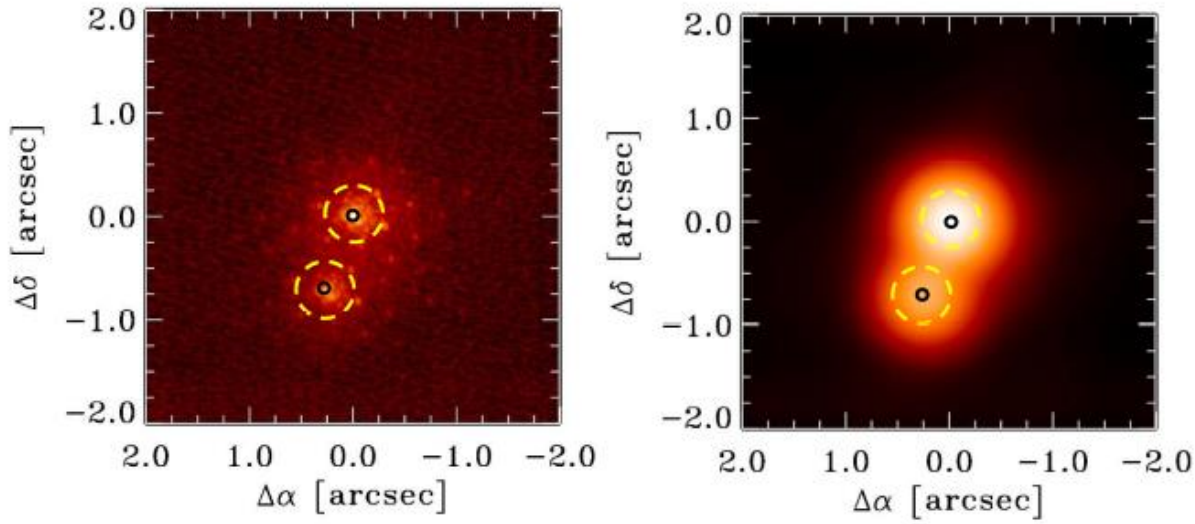

Figure 5: *MODHIS would be able to obtain spectra of both components of K2-288b, an M2/M3 pair separated by 0.65" (50AU) with a 4 MEarth planet. The Keck AO image (left) clearly separates two stars while a 500 mas blurred image (right) suggests the challenge of observing such a system with a seeing-limited spectrometer. The circles represent apertures for seeing-limited (500 mas) and diffraction limited (30 mas) spectrometers.*

1.3.4. Planet Demographics in Binary Systems

MODHIS's diffraction-limited angular resolution will uniquely enable the study of transiting planets in close binaries (<0.5″) which are typically ignored by seeing-limited instruments, (Fig. TBD; Feinstein et al. (2019)). Knowing which star of a pair hosts the planet makes a dramatic difference to the derived planet radius and density (Ciardi et al., 2015) and a demographic study will inform how planet formation proceeds in binary systems, a topic of great theoretical interest (Winn and Fabrycky, 2015; Kraus et al., 2016; Moe and Kratter, 2019).

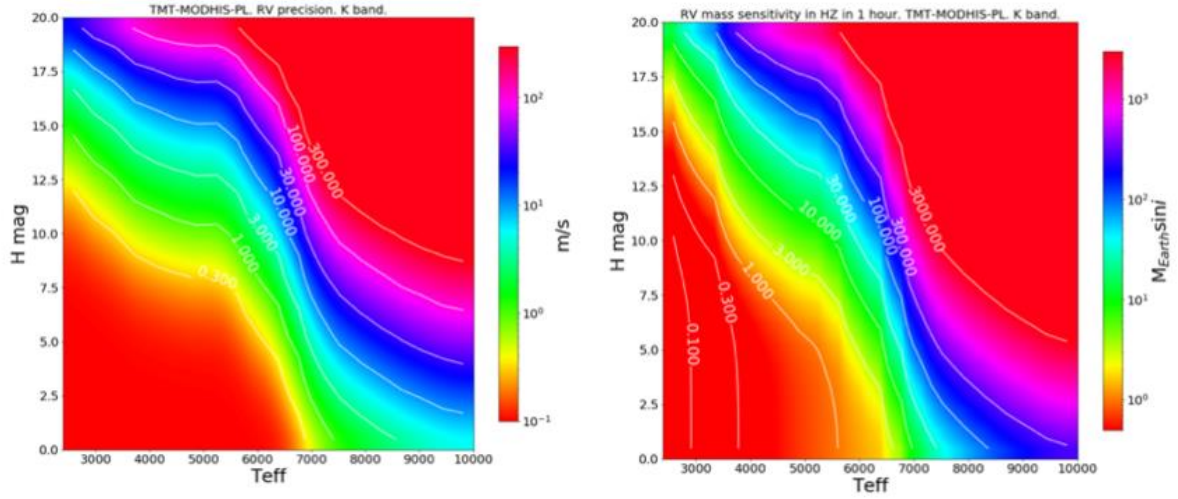

***Figure 6**: Representative single measurement PRV sensitivity in the K band shown in m/s (left) and to exoplanets in the Habitable Zone (right). The plots are given in terms of stellar temperature and H magnitude and reach levels as low as 1 m/s and 1 M_{Earth} for cool stars.*

2. Physics of at the bottom of the main sequence

MODHIS has the potential to revolutionize our understanding of the detailed properties of the coldest stars and brown dwarfs, the late-M, L, T, and Y "ultracool" dwarfs (Kirkpatick 2005). These objects, like their warm exoplanet analogs, have cool atmospheres whose spectral energy distributions, shaped by strong atomic and molecular absorption, peak in the infrared. In addition, as intrinsically faint sources ($L \leq 10^{-4}$ $L_{\odot}$), the accessible population is better suited to individual targeting than broad sky surveys, and are thus ideal targets for MODHIS spectroscopy.

The combination of broad wavelength coverage and high-resolution spectroscopy provided by MODHIS will enable novel investigations into the systemic and atmospheric properties of these objects. The availability of thousands of resolved molecular features across the 1-2.5 μm region will enable PRV measurements (σ_{RV} < 100 m/s) that match the astrometric precision of *Gaia*, providing 3D velocity and 6D coordinate vector measurements for population dynamics studies (Hsu et al. 2022), cluster membership (Gagne et al. 2018), and the identification of so-called "fly-by" stars that have/will have close passings of the Sun (Mamajek et al. 2015). PRV measurements will also enable the first detection of gravitational redshift from ultracool dwarfs (of order 300-700 m/s), whose distinct mass/radius dependence compared to surface gravity ($RV_z \propto M/R$, $g \propto M/R^2$, **Figure 7**) provides an opportunity for direct measurement of the substellar, semi-degenerate mass/radius relationship (Burgasser et al. 2019 - DECADAL). PRV monitoring of resolved (exploiting the high spatial resolution of the Laser Guide Star AO feed) and unresolved ultracool dwarf systems (periods of weeks to years) will provide orbit maps that sample the underlying separation, mass ratio, and eccentricity distributions of these systems, critical for testing low-mass star and brown dwarf formation theories (Konopacky et al. 2010). MODHIS provides a particularly unique opportunity for late-M/L plus T dwarf "spectral binaries" for which both primary and secondary RVs can be captured simultaneously from different parts of the spectrum (Burgasser et al. 2010; Bardalez Gagliuffi et al. 2014).

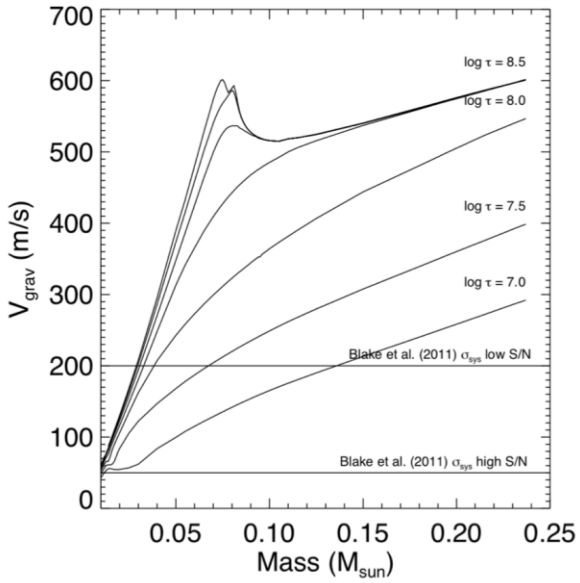

Figure 7: *From Burgasser et al. (2019), the predicted gravitational redshift signal as a function of mass and age (log τ in years). This signal provides a direct probe of the mass and radius of substellar objects, the latter of which is difficult to measure in non-transiting systems. Lines show the current range of RV precision in best-case observations with Keck NIRSPEC. MODHIS will have both the improved sensitivity and RV precision to vastly outperform current measurements, probing this relationship into the planetary mass regime where the targets are quite faint.*

MODHIS spectroscopy will also enable rotational velocity studies of low-mass stars and brown dwarfs in the field and in clusters of various ages, providing new insights into angular momentum evolution as a function of mass and age in the regime of fully convective interiors and neutral atmospheres (Irwin et al. 2011). Such measurements are particularly valuable for samples of photometric variability ultracool dwarfs, increasingly available through facilities such as TESS, (Ricker et al. 2014), SPECULOOS (Delrez et al. 2018), and PINES (Tamburo & Muirhead 2019), as they enable statistical radius measurements and studies of latitudinal structure (Metchev et al. 2015; Vos et al. 2017). In addition, by comparing Zeeman line broadening or splitting of magnetic-sensitive features such as K I (1.24 μm) and FeH (0.98 μm, 1.2 μm, and 1.5 μm) to non-sensitive features, we will be able to directly examine the correlation between magnetic field strength and rotation (Reiners & Basri 2006; Terrien et al. 2022), and potentially map magnetic structures (Zeeman Doppler Imaging; Donati & Brown 1999; Morin et al. 2018, Section 3.2), as empirical tests for dynamo models in the fully-convective regime (Browning 2008; Brown et al. 2020). Spectral monitoring of ultracool stars and brown dwarfs will also provide insights into the 3D structures and dynamics of condensate clouds, which form in both ultracool dwarf and giant exoplanet atmospheres (Charnay et al. 2018). The continuum absorption and scattering opacity of condensates mutes atomic and molecular features, and when these features are monitored in velocity space (line profile variability) it is possible to generate a Doppler imaging map of cloud structures (Crossfield 2014, **Figure 8**). Concurrent monitoring of regions of high and low atmospheric opacity, which sample the upper and lower atmospheres respectively, can be used to build a combined vertical and azimuthal map of cloud structures that can be compared to 3D atmosphere models (Buenzli et al. 2012; Apai et al. 2013; Marley & Robinson 2015).

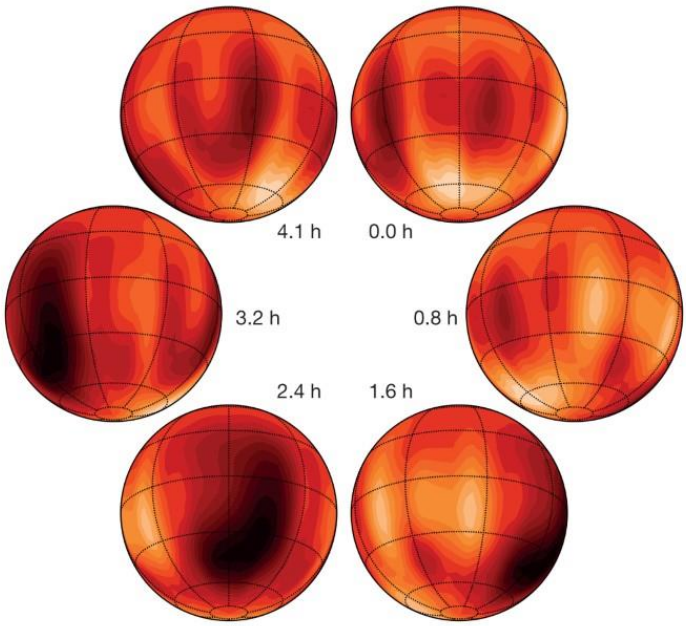

Figure 8: *From Crossfield et al. 2014, a cloud map of the nearby L/T transition brown dwarf Luhman 16B. Using high-resolution K band spectroscopy, the authors were able to map dark and light spots on the surface of the brown dwarf which are likely due to cloud features. Making these types of maps requires high SNR observations of substellar targets, which is challenging for most current 8-10 meter class telescopes beyond the brightest targets like Luhman 16B. With the sensitivity of MODHIS coupled with the light collecting power of TMT, maps such as these should be obtainable for a wide swath of interesting brown dwarfs and potential gas giant planets.*

3. Spectropolarimetry with MODHIS

The design of MODHIS is optimized to provide detailed information on the atmospheres and dynamics of a range of astronomical objects. However, there are unique aspects of characterization that cannot be achieved with typical spectroscopic observations alone. Spectral observations of polarized light offer a unique window into a variety of astronomical phenomena, such as the structure of circumstellar or circumplanetary material, the existence and strength of stellar or planetary magnetic fields, the properties of clouds in planetary atmospheres, or potentially the existence of oceans on terrestrial planets. The current design for MODHIS includes a spectropolarimetry mode, in which polarized light can be measured as a function of wavelength in addition to total intensity light. This capability is ***unique*** amongst the first light suite of instruments for all ELTs. Below is a description of just a few of the potential science cases that can be achieved with MODHIS's spectropolarimetry capability.

3.1. Scattering Processes on Exoplanets

Since a polarization signature is commonly produced by light being scattered, detecting polarized light can uniquely probe the properties of the scattering bodies. On an exoplanet, there are a number of potential scattering sources, such as solids that are parts of aerosols or clouds, or liquids on the planetary surface, that could yield a strongly polarized signal. Given the potential of TMT to detect planets smaller than Jupiter in reflected light, having the capability of exploring their atmospheres and surfaces in depth via spectropolarimetry is a unique opportunity afforded by MODHIS. Here we describe two potentially exciting science cases with MODHIS – the

detection of clouds in large and small planets and the possibility of exploring surface properties of small planets, all with spectropolarimetry.

3.1.1. Probing Clouds in Exoplanet Atmospheres

One of the cornerstone science cases for polarimetry for the two decades has been the detection and characterization of atmospheric condensates, namely clouds, hazes, and/or aerosols. The red colors of brown dwarfs and Jovian-mass companions, coupled with often strong signatures of variability (e.g., Vos et al. 2020), affirm the likely ubiquity of clouds amongst planets like Jupiter. Furthermore, the measurement of a large number of featureless transmission spectra of smaller Neptune-like planets has been attributed to the presence of hazes or aerosols (e.g., Sing et al. 2016). Indeed, all planets in the Solar System with atmospheres harbor condensates of some variety, spanning a range of compositions and properties. At the same time, with current spectral datasets, clouds remain extremely challenging to characterize and model. Clouds are inherently complex, three-dimensional structures, but tend of be approximated as one dimensional, uniform sources of opacity. Part of the complexity stems from the uncertainty in properties such as the composition of the clouds and the distribution of particle sizes in the clouds. These properties can be explored with polarimetry.

Polarized light detected from an L-type brown dwarf was recognized to be likely due to a combination of scattering off atmospheric clouds and either oblateness from rotational broadening or inhomogeneous cloud coverage (Sengupta 2003). Marley & Sengupta (2011) explored this concept in detail in the context of directly imaged exoplanets, finding potential polarized signal strengths of up to 1.5% in the *J* band. In this case, thermal emission from the planet itself is being scattered off the clouds. Recently, the detection of polarized light from the nearby brown dwarf pair Luhman 16AB (Millar-Blanchaer et al. 2020) demonstrated that signals can be very small (<0.1%), but detectable with current instrumentation. Modeling of these two objects has yielded insight into the average cloud size distributions and potential banded structure of the atmosphere, information that is currently impossible to glean from any other measurement. **Figure 9** shows models for Luhman 16AB from Mukherjee et al. (2021).

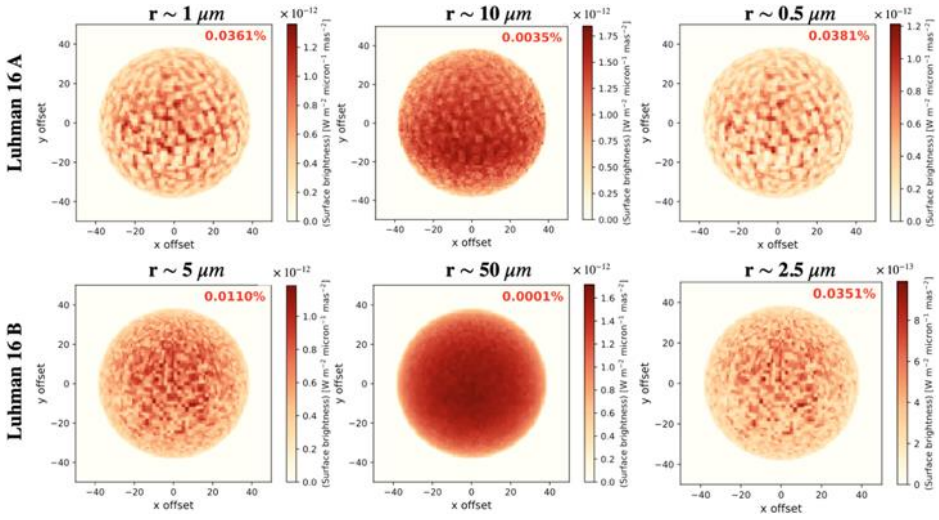

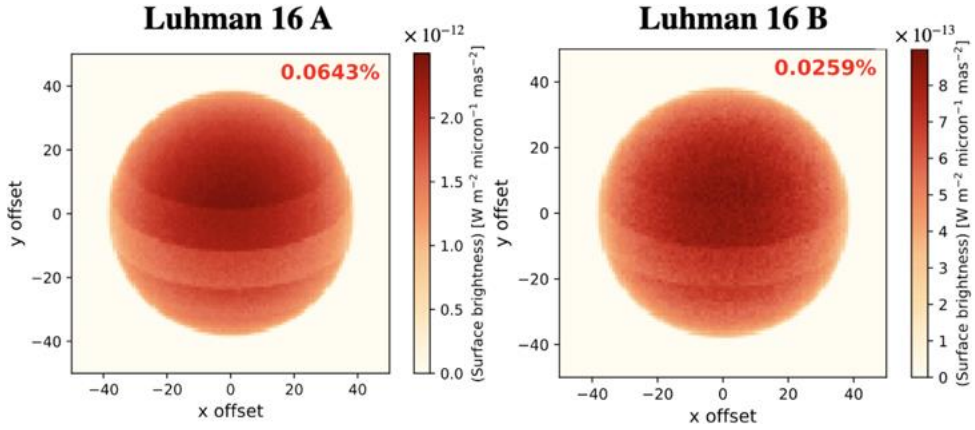

Figure 9: *From Mukherjee et al. (2021), model cloud structures for Luhman 16A and B, coupled with the expected degree of linear polarization from each case. In the top panels, different "typical" grain sizes are considered, generating surface brightness maps for each brown dwarf. The authors conclude that Luhman 16A must have smaller typical cloud grains than Luhman 16B. The bottom panel shows two notional models of cloud banding structure that could generate a polarized light signal. The authors find that banding models tend to produce a higher degree of polarization than measured by Millar-Blancher et al. (2020). Data at additional wavelengths, such as offered by spectropolarimetry, could more tightly constrain these types of models.*

Detection of self-luminous objects like brown dwarfs or young Jovian exoplanets with spectropolarimetry will enable the dramatic expansion of work such as this, which is only based on a single wavelength photometric measurement. Spectra in polarized light probe different atmospheric depths, which enables modeling of the structure of the clouds as a function of scale height. Wavelength-dependent data also provides information about grain composition.

Although the focus of current measurements has been on self-luminous planets, the expectation is that reflected light from a variety of exoplanets will offer constraints of cloud properties. The incoming stellar light could be scattered off of particles in the clouds, and the polarization signal will depend on the nature of the scattering. This behavior is observed in Solar System planets and moons (e.g., Kaydash et al. 2015, West et al. 2015). Recent modeling work has explored the predicted degree of polarization for exoplanets in reflected light given for a range of planet parameters, looking in detail at the type scattering and whether there was single or multiple scattering (e.g., Bailey et al. 2018, Chakrabarty & Sengupta 2021, Sanghavi et al. 2021). The results of these types of models depend strongly on the phase of the orbit and the inclination of the orbital plane, resulting in either no polarization signal at unfavorable observing phases to upwards of 60% polarization fraction in favorable geometries with single scattering. **Figure 10** shows an example of such a calculation from Chakrabarty & Sengupta (2021) for multiple scattering off of a cloud appropriate for a Hot Jupiter (which are also appropriate for young, directly imaged planets and some brown dwarfs), assuming Mie scattering. The calculations are performed in the visible wavelength regime, and are highly wavelength dependent. The expectation is some decrease in polarization degree in the near-infrared bands of MODHIS, suggesting that the blue-arm of MODHIS is more ideal for detection of reflected light polarization signals. The spectroscopic information attainable in conjunction with polarization will provide strong constraints on cloud composition and grain properties. Furthermore, high resolution spectroscopy offers the ability for cross-correlation, which has been shown to be extremely

effective in teasing out faint signals in various data sets (e.g., Wang et al. 2021). The expectation for MODHIS is that spectropolarimetric cross-correlation will be feasible for detecting scattering off of clouds in unresolved planets, such as Hot Jupiters or Hot Neptunes. Thus, this mode of MODHIS provides a unique means to study exoplanet clouds that will not be achievable with other facilities.

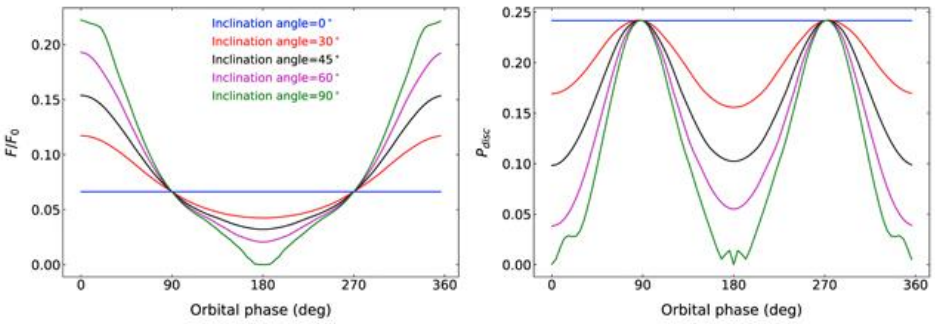

Figure 10: *From Chakrabarty & Sengupta (2021), the albedo (left) and total expected polarization (right) as a function of orbital phase. Different orbital inclinations are represented by different colors. The modeled planet is a cloudy planet with multiple scattering off of cloud particulates expected for Hot Jupiters, consisting primarily of fosterite (Mg_2SiO_4). In all cases, the planet reaches 25% polarization. This calculation was performed at 0.5 um, and at the wavelengths of MODHIS the signal will likely be smaller, but still detectable.*

3.1.2. Polarization Signatures of Molecules, Earthshine and Biosignatures

One of the most exciting opportunities with MODHIS is its potential for detecting and characterizing small worlds, as detailed in Section 1. The spectropolarimetry capability of MODHIS offers the opportunity look in depth at atmospheres and potentially surfaces of these objects, which cannot be achieved by other techniques. This is based on the fact that atmospheric molecules such as water, surface features such as liquid oceans, and even organisms such as grass and trees, polarize light via scattering.

The polarization off of atmospheric molecules (as opposed to condensates) has been explored extensively both for gas giants and for smaller planets. Rayleigh scattering, which we are highly familiar with on Earth, generates among the strongest polarization signals, with models predicting stronger polarization in cloud-free than cloudy atmospheres (e.g., Madhusudhan & Burrows 2012, Karalidi et al. 2013, Chakrabarty & Sengupta 2021, Rossi et al. 2022). **Figure 11** shows an example from Bailey et al. (2018) for the transiting exoplanet HD 189733b, which compares Rayleigh scattering from small atoms and molecules in the atmosphere to scattering off of clouds. Rayleigh scattering offers polarization signals equal to or higher than particulate scattering, and is still significant at long wavelengths.

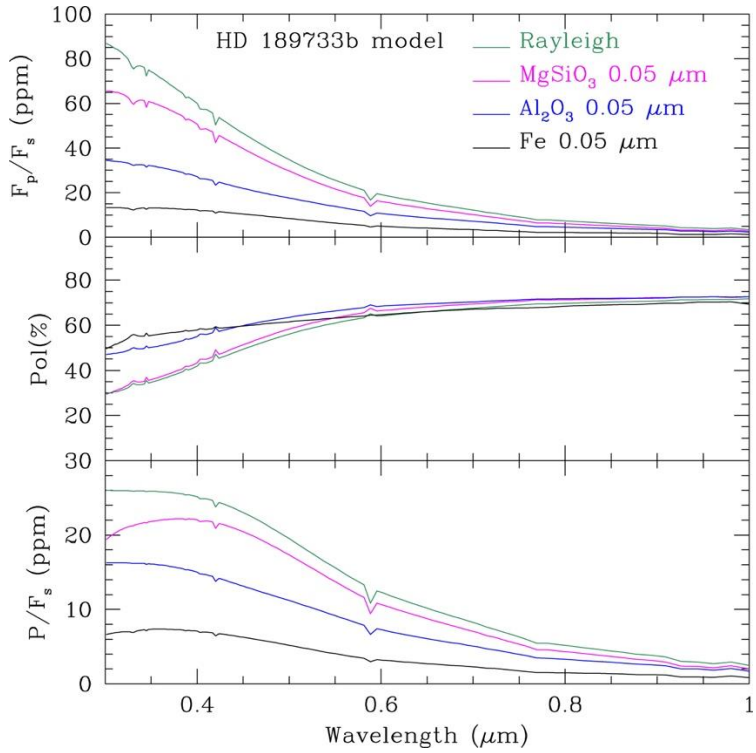

Figure 11: *From Bailey et al. (2018), models of reflected light off of the Hot Jupiter HD 189733b under assumptions of various cloud particles and simple Rayleigh scattering. The top panel shows the reflected light flux divided by the flux from the star. The middle panel shows the percent polarization from the reflected light, and the bottom is the polarization measurement expected in combined light. The polarization percentage is high in all cases, including at the MODHIS wavelength regime near 1 μm. Rayleigh scattering here is modeling by using scattering from H, He, and H_2, and can be measured off of atmospheres regardless of whether clouds are present. This offers the opportunity to characterize the molecular and atomic constituents of atmospheres.*

For terrestrial planets, both Venus and Earth have been studied extensively in polarized light to understand the potential polarization signal from a similar exoplanet. Observations from satellites or of the Moon have provide a detailed look at "earthshine", or the sunlight scattered off the Earth. Miles-Paez et al. (2014) used ground based spectropolarimetry measurements of the earthshine reflection off of the Moon to measure the polarized signal from the Earth across the optical and near-infrared. This is shown in **Figure 12**, and includes the wavelength range covered by MODHIS. While the signal is strongest in the optical, the degree of polarization is above 2% across the whole near-infrared, which a very strong signal in the Y-J band from water and O_2. Indeed, the polarizing properties of water are extremely strong and well-documented (e.g., Stam 2008, Karalidi et al. 2011). This shows that species such O_2 might be more easily found via spectropolarimetry than with traditional absorption line spectroscopy. With MODHIS having the sensitivity to detect these types of planets in transit with NFIRAOS, and potentially via direct imaging with upgraded AO systems like PSI, the capability of spectropolarimetry becomes critical for the goal of characterizing Earth-like worlds.

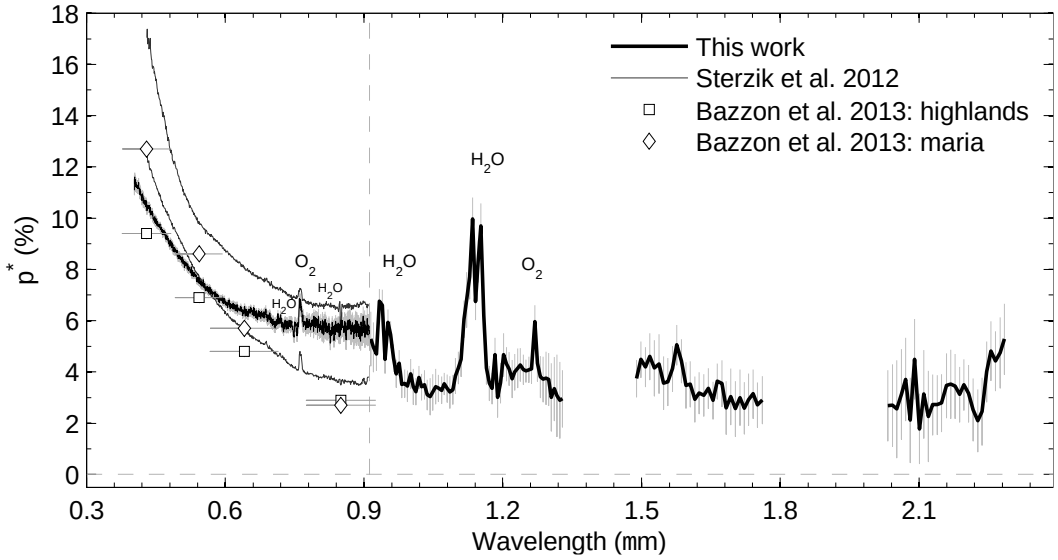

Figure 12: *From Miles-Paez et al. (2014), the polarization fraction of light reflected off of Earth via measurements of earthshine on the Moon. The wavelengths considered cover the full extent of the MODHIS spectral range, and are compared to earlier works in the optical. While polarization signals are the strongest at the shortest wavelengths in the optical, there is polarized light about 2% across the full near-infrared. Additionally, there are particular strong polarization signatures from water and O_2 in the YJ band, or the blue channel of MODHIS, that may be detectable on Earth-like planets harboring these species.*

Spectropolarimetry gets us a step further by offering the ability to probe surface features. For example, Gordon et al. (2023) explored the wavelength-dependent polarimetric signal from surface features on Earth-like planets, including ocean, sand, and trees. The results are shown in **Figure 13**. Oceans strongly polarize light, with up to 70% polarization fraction around ~1-1.2 µm. Ice, forests, sand, and grass are also strongly polarizing, often in similar wavelength regimes. However, combinations of surface features can be distinguished by comparing the ratio of various Stokes parameters. While these results are based only on the Earth, they make a strong argument for the use of spectropolarimetry in future missions focused on biosignature work. Thus, MODHIS has a key role to play in the era of characterization of Earth-like planets and the search for life signs on these worlds.

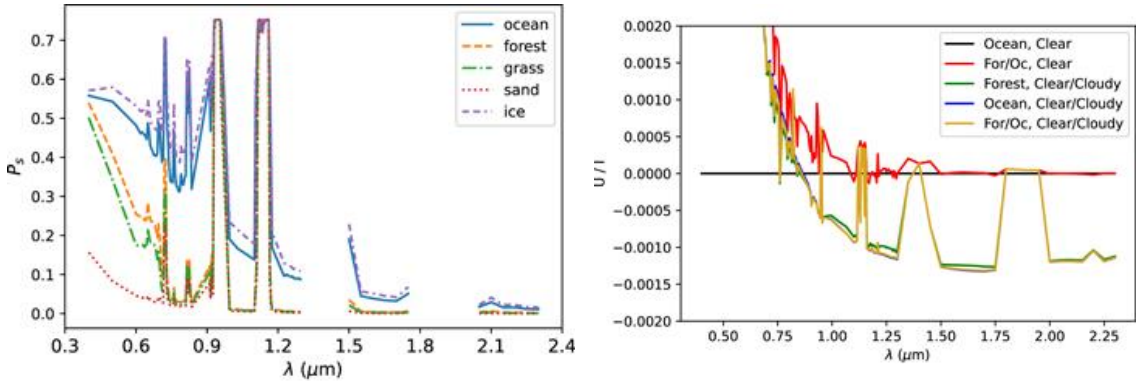

Figure 13: *From Gordon et al. (2023): (**Left**) The polarization fraction as a function of wavelength for a simulated Earth-like planet given a variety of surface compositions at a fixed phase angle. In this case there is a cloud-free atmosphere to visualize the extent of the polarization signal free of the impact of clouds. Strong polarization fractions are generated by oceans and ices across many wavelengths. Sand, forests, and grass have polarization signatures in specific bands, overlapping with water polarization. (**Right**) The relative signal in Stokes U versus total intensity of different terrestrial surface features as a function of wavelength. For ocean-only worlds, there is no signal in U/I, whereas the inclusion or forest or forest/ocean combinations results in a signal that is distinguishable with enough wavelength coverage. Important regimes include the wavelengths covered by MODHIS.*

3.2. Zeeman Doppler Imaging of Planet Host Stars and Giant Planets

Light becomes polarized in the presence of magnetic fields, and thus measurements of polarized light have often been used to infer magnetic field strengths and geometries. Zeeman Doppler imaging takes advantage of this by using spectropolarimetry of rotating stars to map stellar magnetic fields (see a review by Kochukhov 2021). If star spots with different polarizations are rotating across the disk of the star, there will be variation in the line profile in polarized light, much like in the case of Doppler imaging of stellar surfaces (see Section 2). **Figure 14** shows an example of the signal one might expect to see in a spectropolarimetric line measurement due to rotating magnetic spots.

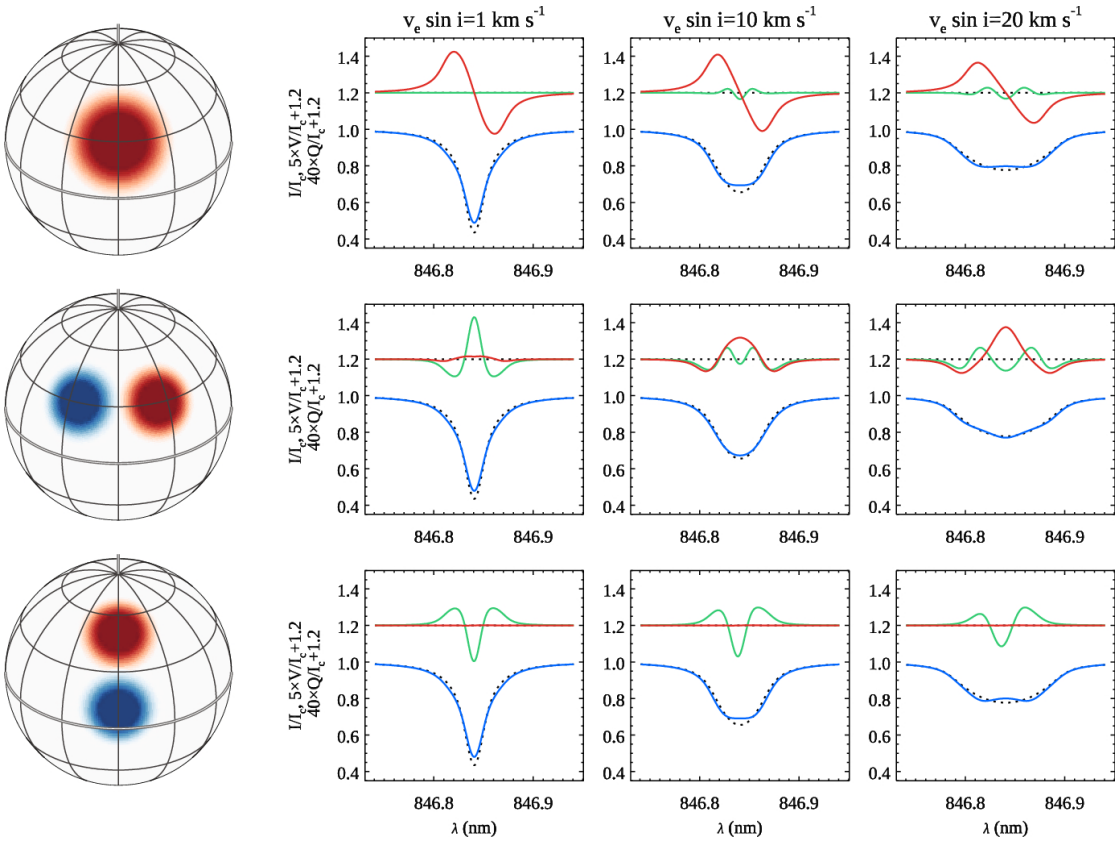

Figure 14: *From Kochukhov (2021), models of the expected signal in polarized light for three notional magnetic field spot geometries. The top row shows a single spot, the middle two*

horizontally separated spots, and the bottom two vertically separated spots. All spots have 3 kG field strengths, and the red and the blue indicate different polarities. The columns show the expected line profiles based on the rotation speed of the source, measured in total intensity (solid blue), Stokes V (red), and Stokes Q (green). The Stokes lines are magnified for clarity, with the V parameters about 8 times stronger than the Q. Current spectropolarimeters regularly measure all four Stokes parameters and detect variations such as these, suggesting that MODHIS could do the same with proper instrumental calibration.

Data collected previously with other spectropolarimeters such as HARPSpol, SPIRou, ESPaDOnS, and others have yielded fascinating insights on the magnetic field topology of a variety of stellar types (e.g., Wade et al. 2000, Donati et al. 2006, Kochukhov et al. 2013, Rosén et al. 2015, Klein et al. 2021a,b, Williamo et al. 2022). The data and models have shown that the signal is stronger in circularly polarized light (Stokes V) than in linearly polarized light (Stokes Q and U). The latter is what we plan to measure with MODHIS (expected signals are <1%). However, recent work (e.g., Rosén et al. 2015) has shown that a signal is indeed present in Stokes Q and U on low mass sources, and is needed to fully explore the magnetic fields of these stars, as degeneracies occur when only circularly polarized light is measured. Thus, measuring linear polarization variations for active stars can still yield valuable information about the magnetic field, albeit with much smaller signals.

The science goals of Zeeman Doppler imaging for MODHIS are two-fold. First, as the only spectropolarimeter available at first like on the ELTs, MODHIS will be unique in its ability to map the magnetic field properties of faint, low mass stars that host terrestrial planets. Since the sizes of the Zeeman variation are small, very high SNR is required in individual spectra, which must be obtained only over a few rotation periods to capture the magnetic field information before it changes significantly. Thus, high SNR in fairly short exposures is required. Only MODHIS will have the ability to obtain such spectra, which will be critical for assessing the likely impact of magnetic activity on the terrestrial planets in these systems. Given the high occurrence rate of small planets around M-type stars, magnetic activity has been highlighted as a major factor impacting habitability on these worlds (e.g., Khodachenko et al. 2007, Luger & Barnes 2015, Kislyakova et al. 2017, Ridgway et al. 2023). However, we still lack a complete understanding of the origin and structure of these fields, especially on the smallest stars (e.g., Browning et al. 2016). Zeeman Doppler imaging with MODHIS will offer the first opportunity to map, for example, the magnetic field on systems such as TRAPPIST-1. An example of a magnetic field map for the planet host Proxima Cen is shown in **Figure 15**, derived by Klein et al. (2021b) using HARPSpol. In addition to exploring questions of habitability, maps such as these provide detailed insight on the physics of low mass stars.

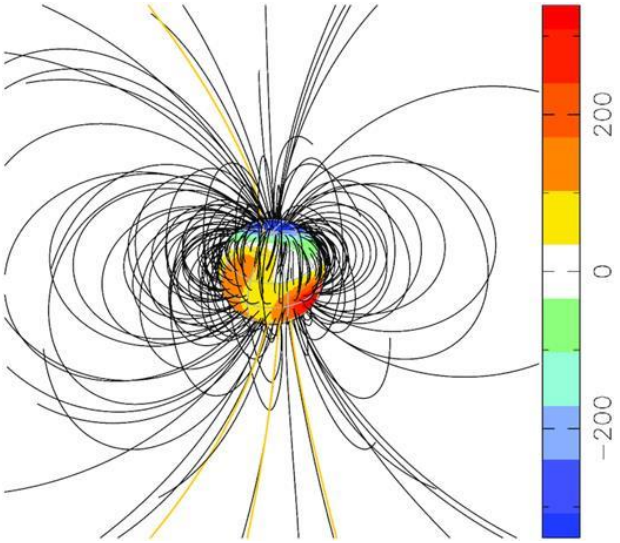

Figure 15: *From Klein et al. (2021b), the reconstructed magnetic field map for Proxima Cen, the closest star to the Sun, which hosts a potentially habitable planet. This M5.5 star has a known magnetic activity cycle, and the close separation of the planet (~0.05 AU) means that its habitability is likely impacted by the stellar magnetic field. This map was made using Zeeman Doppler imaging, which is a goal science area for MODHIS's spectropolarimetry mode. Using this technique, Klein et al. (2021b) find a magnetic field strength of 200 G, that the field is poloidal, and that the planet, Proxima b, is likely outside of the region of direct magnetic interactions with the star. With MODHIS, we will be able to generate maps for even smaller and/or more distant worlds with potentially habitable planets.*

The second goal of Zeeman Doppler imaging with MODHIS will be to create the first magnetic field maps for gas giant exoplanets. Bright, massive planets like Beta Pictoris b or HR 8799 bcde are amenable to high SNR spectropolarimetric observations, but are inaccessible with current facilities because of the need for AO and high-contrast techniques. MODHIS naturally fills this niche with its fundamental design as a high-contrast instrument fed by AO (e.g., Plummer & Wang 2023). Magnetic fields are found in the gas giants in our Solar System such as Jupiter, but have not been definitively measured on any other exoplanets. Beyond simple detection of magnetic activity, MODHIS will be able to explore the structure of the magnetic field and therefore provide hints about the interiors of these planets. This will also shed light on possible interactions between the magnetic field of the planet and orbiting moons, such as those observed between Jupiter and Io that give rise to aurora on Jupiter (e.g., Khurana et al. 2004).

3.3. Spectropolarimetry of Circumplanetary Disks

Disk material surrounding young stars is well-known to be often strongly polarized due to the non-spherical symmetry of a disk and the scattering properties of grains (e.g., Williams & Cieza 2011). The same is likely to be true for circumplanetary material. It is widely expected that gas giant planets will form an accretion disk similar to the circumstellar disk from which they form, as evidenced by the significant number of large, coplanar moons around the Solar System gas giants (Barr 2016). While the hunt for exomoons is already taking place (see Sections 1.3.3 and 3.3 above), much can be learned about the processes that form both gas giants and the moons by exploring the disks from which they feed and form. Therefore, detecting and characterizing

circumplanetary disks is an exciting area of study that will be of great interest to TMT. As of writing (2023), there are a few confirmed and/or candidate circumplanetary disks that have been detected via detection of emission lines from accretion (e.g., Sallum et al. 2015, Wagner et al. 2018, Zhou et al. 2022, Follette et al. 2023). While such measurements are powerful, they do not provide information about the structure or composition of the disk. Additional information can be gleaned from spectral energy distributions, which probe temperatures, compositions, and grain sizes. However, when fitting an SED, this information is degenerate. Information about the scattering properties of the grains via polarization measurements helps break these degeneracies (e.g., Esposito et al. 2020).

Recent work has explored the potential detectability of circumplanetary disks in polarized light. Szulágyi & Garufi (2021) explored the possibility of imaging polarized light in the J band, varying parameters such as planet mass and disk inclination. They generated mock images of the expected polarization signal, which are shown in **Figure 16**. The authors find that circumplanetary disks are detectable in polarized light for a number of configurations, particularly around high mass planets. Importantly, they also find that their signals are distinguishable from the circumstellar disk, which is likely present concurrently with the disk around the planet. The strength of the signal ranges from 1.5 – 3.2%, higher than some of the brightest circumstellar disks due potential for a strong accretion-shock surface on the planet.

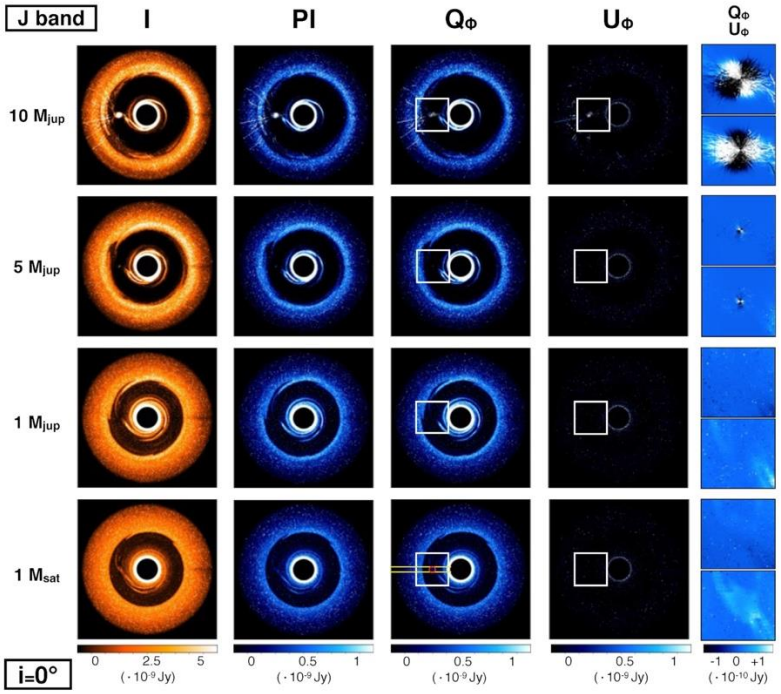

Figure 16: *From Szulágyi & Garufi (2021), simulated polarized scattered light images at J band of a circumplanetary disk assuming 0° inclination (face-on) and a distance of 100 pc. Columns demonstrate the brightness of the disk in total intensity and then in various Stokes parameter channels.*

Since the disks are expected to be spatially small (~0.2 AU, which is ~1 mas at the distance of nearby star forming regions), polarimetric imaging that maps the geometry of circumstellar disks

is unlikely to be feasible for circumplanetary disks. However, the compactness of these disks and strength of the polarized signal makes them prime candidates for MODHIS's spectropolarimetry mode. Disk spectropolarimetry can be used to determine aspects of a disks geometry and structure that cannot be probed by imaging alone. For instance, spectropolarimetry can be used to map the rotational structure of the disk and determine whether or not an inner hole is present (e.g., Vink et al. 2005). It can be used to assess the location and strength of accretion by constraining the extent of the emission region of emission lines, and probe potential disk compositional information. An ideal use of MODHIS would be deep observations in spectropolarimetry mode of known young gas giants to fully characterize the nature of their disks and probe exomoon formation.

3.4. Exomoon Detection in Polarized Light

Exomoon detection and characterization will be a primary science case for MODHIS, as described in Section 1.3.3. The spectropolarimetric capabilities of MODHIS will allow for a particularly unique method of exomoon detection – variation in the polarimetry signal during the transit of an exomoon. The idea is somewhat analogous to the well-known Rossiter-McLaughlin effect measured with typical Doppler spectroscopy. The transiting body blocks part of the light of its host, yielding a change in the integrated signal from that host. In the case of a rotating giant planet, the light may be polarized due to scattering off atmospheric clouds (Section 3.1). If part of the light from the planet is blocked due to a transiting exomoon, an asymmetry in the polarimetric signal would be generated, yielding a net polarized signal that could be detectable with MODHIS in spectropolarimetry mode.

This idea was explored in detail in Sengupta & Marley (2016). They used models of the potential polarized signal of a spherical planet when blocked by a large body in transit to predict the expected percent polarization of the planet. The results of one of their simulations is shown in **Figure 17** for *J*-band light. Depending on the temperature and gravity of the planet, which impacts the cloud composition and depth, the expected degree of polarization is as high as 0.3%. While this signal is small, it is potentially detectable with MODHIS. This signal was explored for the case of photometric detection only, and future work is needed to determine whether spectroscopic information would be particularly valuable (as in the case of the Rossiter-McLaughlin effect).

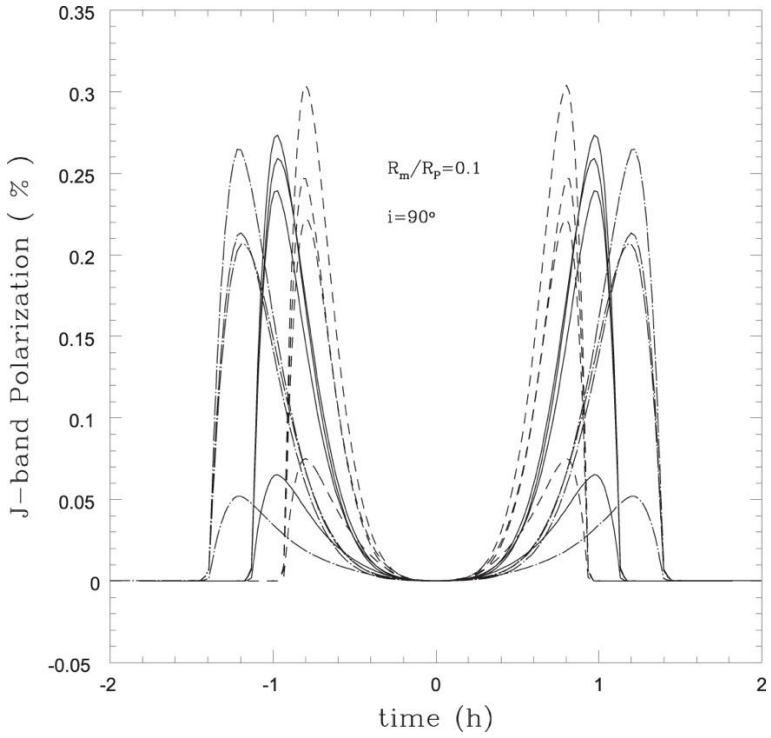

Figure 17: *From Sengupta & Marley (2016), predicted polarization signal variation during the transit of a large exomoon around a gas giant planet. The different curves represent varying parameters of the planet. The solid lines show results for a low surface gravity planet (g=56 m s^{-2}) and temperatures between 600 K – 1200 K. The dashed lines consider the same temperatures, but now g=100 m s^{-2}. The largest signals are around 0.3% polarization fraction, which should be detectable with MODHIS given the current requirements.*

We note that this a similar measurement has been attempted before with success in a slightly different context. Miles-Paez et al. (2019) obtained measurements of the TRAPPIST-1 system in polarized light during the transits of three of its terrestrial planets. Their results are summarized in **Figure 18**. They detected no polarization signal out of transit, but found a net polarization during the transits, with a peak around 0.1% polarization for TRAPPIST-1d. This indicates that the M8 host star in TRAPPIST-1 is indeed a cloudy object (which is expected for this spectral type). This therefore validates the utility of this technique for measuring polarized light during transits when the host star typically has an undetectable polarization signal. It also suggests the area of polarized signals during transits is ripe for additional theoretical work and modeling.

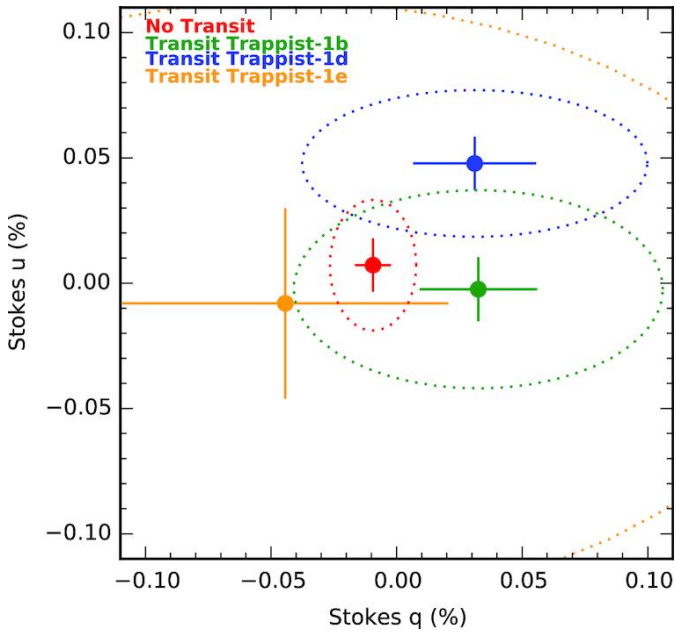

Figure 18*: From Miles-Paez et al. (2019), the measured Stokes U and Q values during the transits of three of the TRAPPIST-1 planets. When no transit is occurring, minimal signal is detected (red). Measurable polarization is detected during the transits of TRAPPIST-1d, with some hints of signals duering the transits of TRAPPIST-1b and 1e. This is likely due to having more data around the transit of TRAPPIST-1d. The signal of ~0.1% is consistent with the predictions of Sengupta (2016).*

3.5. Spectropolarimetry of Nearby AGN

Polarimetric observations of the immediate vicinty of supermassive black holes (SMBHs) have yielded powerful insights into their properties. As in the case of disks around stars, accretion disks in the vicinity of black holes can also scatter photons, resulting in significant polarization of the signal from this material. Indeed, detection of polarized light was able to elucidate and confirm models explaining the difference between type 1 and type 2 Seyfert galaxies (**Figure 19**, e.g., Popovic et al. 2022). Measuring time delay between polarized and unpolarized light can provide a map of the structure of the accretion disks (aka polarimetric reverberation mapping, e.g., Gaskell et al. 2012, Rojas Lobos et al. 2020). Detailed modeling of the polarization signal of blazars, which harbor highly polarized, relativistic jets, can allow for the constraint of both the the accretion disk and the magnetic properties, such as the strength and ordering of the magnetic field (e.g., Schutte et al. 2022). Detailed modeling of the accretion disks with polarimetry may also provide additional constraints on the masses of the SMBHS (e.g., Savic et al. 2018).

Polarization can also be used to detect binary SMBHs, as their orbits are often not circular and thus generate a periodic polarization signal due to the orbital asymmetry (Dotti et al. 2022). Such objects are difficult to find observationally, but are critically important for correlating with gravitational wave signatures and understanding the growth of black holes in galaxy centers.

For bright, nearby AGN, MODHIS can detect and characterize the polarized light coming from the central region, which can be well-localized due to the exquisite spatial resolution provided by TMT+NFIRAOS. Though much of the previous literature has focused on optical polarization

measurements, there are ample lines in the near-infrared that can be used to study the behavior and environs of the SMBHS (e.g., Friedrich et al. 2010). Additionally, the polarization fraction declines by only a few percent between the optical and near-infrared for both the non-thermal sources of emission and thermal emission from the accretion disk (e.g., Bailey et al. 1981).

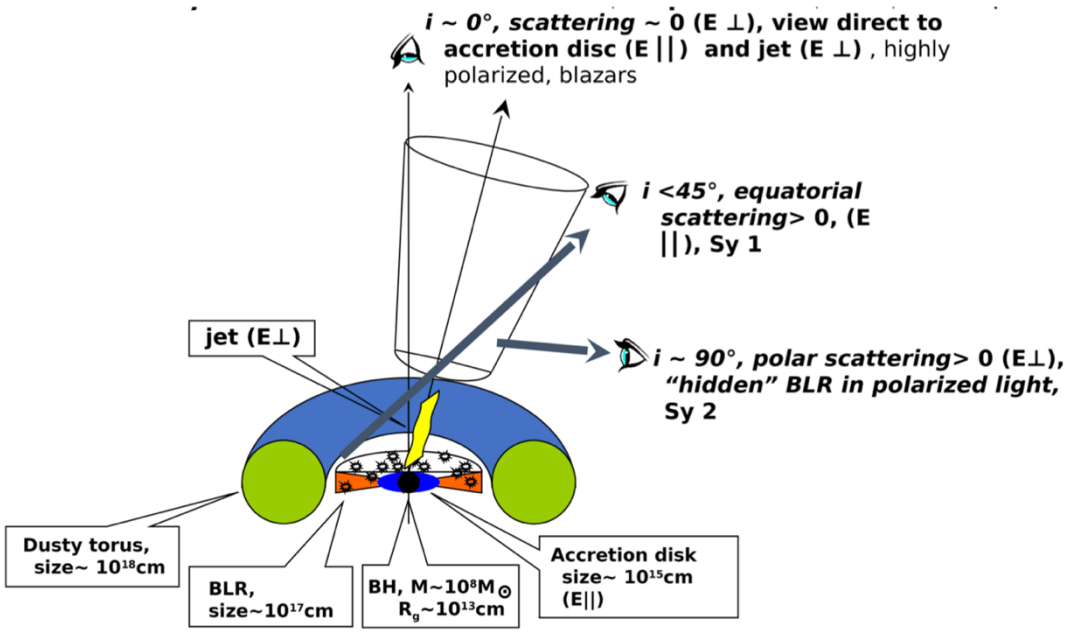

***Figure 19**: From Popovic et al. (2022), a schematic describing the polarization signal seen around AGN as a function of viewing angle. BLR stands for broad line region. The drawing shows the widely accepted model of a torus surrounding the accretion disk of the AGN. The torus is dusty, and thus produces a polarized signal. The polarization signal as a function of Seyfert-type (Sy I or II) solidified the unified model of AGN.*

3.6. Summary of Polarimetry Science Cases and Signals

Here we present a summary of the potential polarimetry science case described above and the strength of the expected polarimetry signal. These signal strengths are relevant for the required polarimetric precision of MODHIS. Note that in some cases involving exoplanets, the targets will be off-axis directly imaged planets, which in other cases the targets will be blended light (transiting or non-transiting) planets. The magnitude range reflects both options when both are possible modes of detection.

Science Case	Linear or Circular?	Bands	Typical Target Mag. (J)	High Contrast?	Time variable?	Polarization Signal
Exoplanet Clouds	Linear	Y and J	~14-17	Yes and No	Yes	Typically ~1% (up to 60%)

Earthshine, Molecules, and Biosignatures	Linear	J	~5-25	Yes and No	No	Typically ~1-3% (up to 70%)
Zeeman Doppler Imaging	Circular and Linear	J	~5-15	Yes and No	Yes	~1%
Circumplanetary Disks	Linear	Y and J	~13-18	Yes	No	~1 – 3%
Exomoons	Linear	Y and J	~5-15	Yes and No	Yes	0.3%
AGN	Circular and Linear	Y and J	~10-15	No	Yes	~1-5%

Table 1: Summary information for polarimetry science cases.

References:

Bailey, J., Cunningham, E.C., Hough, J.H., Axon, D.J. (1981), MNRAS, 197, 627

Bailey, J., Kedziora-Chudczer, L., Bott, K. (2018), MNRAS, 480, 1613

Barr, A.C. (2016), Astronomical Review, 12, 24

Batygin K (2018) AJ, 155(4):178.

Batygin, K., Morbidelli, A. (2020), ApJ, 894, 143

Beatty TG, Marley MS, Gaudi BS, Colón KD, Fortney JJ and Showman AP (2019) AJ, 158(4):166.

Beltz H, Rauscher E, Brogi M and Kempton EMR (2021) AJ, 161(1):1.

Birkby JL (2018) arXiv e-prints, arXiv:1806.04617.

Birkby JL, de Kok RJ, Brogi M, de Mooij EJW, Schwarz H, Albrecht S and Snellen IAG (2013) MNRAS, 436:L35–L39.

Birkby JL, de Kok RJ, Brogi M, Schwarz H and Snellen IAG (2017) AJ, 153(3):138.

Birkby JL, de Kok RJ, Brogi M, de Mooij EJW, Schwarz H, Albrecht S and Snellen IAG (2013) MNRAS, 436:L35–L39.

Bourrier V, Lovis C, Beust H, Ehrenreich D, Henry GW, Astudillo-Defru N, Allart R, Bonfils X, Ségransan D, Delfosse X, Cegla HM, Wyttenbach A, Heng K, Lavie B and Pepe F (2018) Nature, 553(7689):477–480.

Bowler B, Sallum S, Boss A, Brandt T, Briesemeister Z, Bryan M, Crepp J, Currie T, Fortney J, Girard J, Jensen-Clem R, Kama M, Kraus A, Konopacky Q, Liu M, Marley M, Mawet D, Meshkat T, Meyer M, Morley C, Skemer A, Wang J, Wu YL, Close L, Marois C and Nielsen E (2019), BAAS, 51, 496.

Brogi M, de Kok RJ, Albrecht S, Snellen IAG, Birkby JL and Schwarz H (2016) ApJ, 817(2):106.

Brogi M, de Kok RJ, Albrecht S, Snellen IAG, Birkby JL and Schwarz H (2016) ApJ, 817(2):106.

Brogi M, Line M, Bean J, Désert JM and Schwarz H (2017) ApJ, 839(1):L2.

Brogi M and Line MR (2019) AJ, 157(3):114.

Brogi M, Snellen IAG, de Kok RJ, Albrecht S, Birkby J and de Mooij EJW (2012) Nature, 486:502–504.

Brogi M, Snellen IAG, de Kok RJ, Albrecht S, Birkby JL and de Mooij EJW (2013) ApJ, 767:27.

Browning, M.K., Weber, M.A., Chabrier, G., Massey, A.P. (2016), ApJ, 818, 189

Canup, R.M., Ward, W.R. (2006), Nature, 441, 834

Carleo I, Benatti S, Lanza AF, Gratton R, Claudi R, Desidera S, Mace GN, Messina S, Sanna N, Sissa E, Ghedina A, Ghinassi F, Guerra J, Harutyunyan A, Micela G, Molinari E, Oliva E, Tozzi A, Baffa C, Baruffolo A, Bignamini A, Buchschacher N, Cecconi M, Cosentino R, Endl M, Falcini G, Fantinel D, Fini L, Fugazza D, Galli A, Giani E, González C, González-Álvarez E, González M, Hernandez N, Hernandez Diaz M, Iuzzolino M, Kaplan KF, Kidder BT, Lodi M, Malavolta L, Maldonado J, Origlia L, Perez Ventura H, Puglisi A, Rainer M, Riverol L, Riverol C, San Juan J, Scuderi S, Seemann U, Sokal KR, Sozzetti A and Sozzi M (2018) A&A, 613:A50.

Chakrabarty, A., Sengupta, S. (2021), ApJ, 917, 83

Ciardi DR, Crossfield IJM, Feinstein AD, Schlieder JE, Petigura EA, David TJ, Bristow M, Patel RI, Arnold L, Benneke B, Christiansen JL, Dressing CD, Fulton BJ, Howard AW, Isaacson H, Sinukoff E and Thackeray B (2018) AJ, 155:10.

Cridland AJ, van Dishoeck EF, Alessi M and Pudritz RE (2020) A&A, 642:A229.

Crossfield IJM (2014) A&A, 566:A130.

David TJ, Contardo G, Sandoval A, Angus R, Lu YL, Bedell M, Curtis JL, Foreman-Mackey D, Fulton BJ, Grunblatt SK and Petigura EA (2021) AJ, 161(6):265.

David TJ, Mamajek EE, Vanderburg A, Schlieder JE, Bristow M, Petigura EA, Ciardi DR, Crossfield IJM, Isaacson HT, Cody AM, Stauffer JR, Hillenbrand LA, Bieryla A, Latham DW, Fulton BJ, Rebull LM, Beichman C, Gonzales EJ, Hirsch LA, Howard AW, Vasisht G and Ygouf M (2018) AJ, 156:302.

de Kok RJ, Birkby J, Brogi M, Schwarz H, Albrecht S, de Mooij EJW and Snellen IAG (2014) A&A, 561:A150.

Dodson-Robinson SE, Veras D, Ford EB and Beichman CA (2009) ApJ, 707(1):79–88.

Donati, J.-F., Howarth, I.D., Jardine, M.M., Petit, P., Catala, C., Landstreet, J.D., Bouret, J.-C., Alecian, E., Barnes, J.R., Forveille, T., Paletou, F., Manset, N. (2006), MNRAS, 370, 629

Dotti, M., Bonetti, M., D'Orazio, D.J., Haiman, Z., Ho, L.C (2022), MNRAS, 509, 212

Duchêne G, Feng YK, Fitzgerald MP, Fortney J, Freedman RS, Knutson H, Konopacky Q, Lilley S, Liu MC, Lopez R, Lupu R, Marley MS, Meshkat T, Miles B, Millar-Blanchaer M, Ragland S, Roy A, Ruane G, Sappey B, Schofield T, Weiss L, Wetherell E, Wizinowich P and Ygouf M (2021) AJ, 162(4):148.

Echeverri D, Ruane G, Jovanovic N, Mawet D and Levraud N (2019) Optics Letters, 44:2204.

Ehrenreich D, Lovis C, Allart R, Zapatero Osorio MR, Pepe F, Cristiani S, Rebolo R, Santos NC, Borsa F, Demangeon O, Dumusque X, González Hernández JI, Casasayas-Barris N, Ségransan D, Sousa S, Abreu M, Adibekyan V, Affolter M, Allende Prieto C, Alibert Y, Aliverti M, Alves D, Amate M, Avila G, Baldini V, Bandy T, Benz W, Bianco A, Bolmont É, Bouchy F, Bourrier V, Broeg C, Cabral A, Calderone G, Pallé E, Cegla HM, Cirami R, Coelho JMP, Conconi P, Coretti I, Cumani C, Cupani G, Dekker H, Delabre B, Deiries S, D'Odorico V, Di Marcantonio P, Figueira P, Fragoso A, Genolet L, Genoni M, Génova Santos R, Hara N, Hughes I, Iwert O, Kerber F, Knudstrup J, Landoni M, Lavie B, Lizon JL, Lendl M, Lo Curto G, Maire C, Manescau A, Martins CJAP, Mégevand D, Mehner A, Micela G, Modigliani A, Molaro P, Monteiro M, Monteiro M, Moschetti M, Müller E, Nunes N, Oggioni L, Oliveira A, Pariani G, Pasquini L, Poretti E, Rasilla JL, Redaelli E, Riva M, Santana Tschudi S, Santin P, Santos P, Segovia Milla A, Seidel JV, Sosnowska D, Sozzetti A, Spanò P, Suárez Mascareño A, Tabernero H, Tenegi F, Udry S, Zanutta A, Zerbi F (2020) Nature, 580(7805):597–601.

Esposito, T.M., Kalas, P., Fitzgerald, M.P., Millar- Blanchaer, M.A., Duchêne, G., Patience, J., Hom, J., Perrin, M.D., De Rosa, R.J., Chiang, E., Czekala, I., Macintosh, B., Graham, J.R., Ansdell, M., Arriaga, P., Bruzzone, S., Bulger, J., Chen, C.H., Cotten, T., Dong, R., Draper, Z.H., Follette, K.B., Hung, L.-W., Lopez, R., Matthews, B.C., Mazoyer, J., Metchev, S., Rameau, J., Ren, B., Rice, M., Song, I., Stahl, K., Wang, J., Wolff, S., Zuckerman, B., Ammons, S.M., Bailey, V.P., Barman, T., Chilcote, J., Doyon, R., Gerard, B.L., Goodsell, S.J., Greenbaum, A.Z., Hibon, P., Hinkley, S., Ingraham, P., Konopacky, Q., Maire, J., Marchis, F., Marley, M.S., Marois, C., Nielsen, E.L., Oppenheimer, R., Palmer, D., Poyneer, L., Pueyo, L., Rajan, A., Rantakyrö, F.T., Ruffio, J.-B., Savransky, D., Schneider, A.C., Sivaramakrishnan, A., Soummer, R., Thomas, S., Ward-Duong, K., (2020), AJ, 160, 24

Fernandes RB, Mulders GD, Pascucci I, Mordasini C and Emsenhuber A (2019) ApJ, 874(1):81.

Flowers E, Brogi M, Rauscher E, Kempton EMR and Chiavassa A (2019) AJ, 157(5):209.

Follette, K.B., Close, L.M., Males, J.R., Ward-Duong, K., Balmer, W.O., Redai, J.A., Morales, J., Sarosi, C., Dacus, B., De Rosa, R.J., Garcia Toro, F., Leonard, C., Macintosh, B., Morzinski, K.M., Mullen, W., Palmo, J., Saitoti, R.N., Spiro, E., Treiber, H., Wagner, K., Wang, J., Wang, D., Watson, A., Weinberger, A.J., (2023), AJ, 165, 225

Fortney, J.J., Marley, M.S., & Barnes, J.W. (2007), ApJ 659, 1661.

Fortney JJ, Marley MS, Saumon D and Lodders K (2008) ApJ, 683(2):1104–1116.

Friedrich, S., Davies, R.I., Hicks, E.K.S., Engel, H., Müller-Sánchez, F., Genzel, R., Lacconi, L.J., (2010), A&A, 519, 79

Fulton BJ, Petigura EA, Howard AW, Isaacson H, Marcy GW, Cargile PA, Hebb L, Weiss LM, Johnson JA, Morton TD, Sinukoff E, Crossfield IJM and Hirsch LA (2017) AJ, 154(3):109.

Gaidos E, Hirano T, Beichman C, Livingston J, Harakawa H, Hodapp KW, Ishizuka M, Jacobson S, Konishi M, Kotani T, Kudo T, Kurokawa T, Kuzuhara M, Nishikawa J, Omiya M, Serizawa T, Tamura M, Ueda A and Vievard S (2022) MNRAS, 509(2):2969–2978.

Gandhi S, Brogi M and Webb RK (2020) MNRAS, 498(1):194–204.

Gao P, Thorngren DP, Lee GKH, Fortney JJ, Morley CV, Wakeford HR, Powell DK, Stevenson KB and Zhang X (2020) Nature Astronomy, 4:951–956.

Gaskell, C.M., Goosmann, R.W., Merkulova, N.I., Shakhovskoy, N.M, Shoji, M. (2012) ApH, 749, 148

Gordon, K.E., Karalidi, T., Bott, K.M., Miles-Páez, P.A., Mulder, W., Stam, D.M. (2023), ApJ, 945, 166

Harada CK, Kempton EMR, Rauscher E, Roman M and Brinjikji M (2019) arXiv e-prints, arXiv:1912.02268.

Hoeijmakers HJ, Schwarz H, Snellen IAG, de Kok RJ, Bonnefoy M, Chauvin G, Lagrange AM and Girard JH (2018) A&A, 617:A144.

Hood CE, Fortney JJ, Line MR, Martin EC, Morley CV, Birkby JL, Rustamkulov Z, Lupu RE and Freedman RS (2020) AJ, 160(5):198.

Johns-Krull CM, McLane JN, Prato L, Crockett CJ, Jaffe DT, Hartigan PM, Beichman CA, Mahmud NI, Chen W, Skiff BA, Cauley PW, Jones JA and Mace GN (2016) ApJ, 826:206.

Karalidi, T., Stam, D.M., Guirado, D. (2013) A&A, 555, 127

Karalidi, T., Stam, D.M., Hovenier, J.W. (2011) A&A, 530, 69

Kaydash, V., Shkuratov, Y., Wolff, M, Videen, G. (2015), "Terrestrial Planets", Polarimetry of Stars and Planetary Systems, 289

Khodachenko, M.L., Ribas, I., Lammer, H., Griebmeier, J.-M., Leitner, M., Selsis, F., Eiroa, C., Hanslmeier, A., Biernat, H.K., Farrugia, C.J., Rucker, H.O. (2007) Astrobiology, 7, 167

Khurana, K.K., Kivelson, M., Vasyliunas, V., Krupp, N., Woch, J., Lagg, A., Mauk, B.H., Kurth, W.S. (2004), "The configuration of Jupiter's magnetosphere", Jupiter: The planet, satellites, and magnetosphere. 593-616

Kipping, D., Bryson, S., Burke, C., Christiansen, J., Hardegree-Ullman, K., Quarles, B., Hansen, B., Szulágyi, J., Teachey, A. (2022), Nature Astronomy, 6, 367

Kislyakova, K.G., Noack, L., Johnstone, C.P., Zaitsev, V.V., Fossati, L., Lammer, H., Khodachenko, M.L., Odert, P., Güdel, M., (2017) Nature Astronomy, 1, 878

Klein B, Donati JF, Moutou C, Delfosse X, Bonfils X, Martioli E, Fouqué P, Cloutier R, Artigau É, Doyon R, Hébrard G, Morin J, Rameau J, Plavchan P and Gaidos E (2020) arXiv e-prints, arXiv:2011.13357.

Klein, B. Donati, J.-F., Moutou, C., Delfosse, X., Bonfils, X., Martioli, E., Fouqué, P., Cloutier, R., Artigau, É., Doyon, R., Hébrard, G., Julien, M., Rameau, J., Plavchan, P., Gaidos, E. (2021a), MNRAS, 502, 188

Klein, B., Donati, J.-F., Hébrard, É.M., Zaire, B., Folsom, C.P., Morin, J., Delfosse, X., Bonfils, X. (2021b), MNRAS, 500, 1844

Kochukhov, O., Alentiev, D., Ryabchikova, T., Boyko, S., Cunha, M., Tsymbal, V., Weiss, W. (2013) MNRAS, 431, 2808

Kochukhov, O. (2021), A&Arv, 29, 1

Kreidberg L, Bean JL, Désert JM, Benneke B, Deming D, Stevenson KB, Seager S, Berta-Thompson Z, Seifahrt A and Homeier D (2014) Nature, 505(7481):69–72.

Lazzoni, C.; Zurlo, A., Desidera, S., Mesa, D., Fontanive, C., Bonavita, M., Ertel, S., Rice, K., Vigan, A., Boccaletti, A., Bonnefoy, M., Chauvin, G., Delorme, P., Gratton, R., Houllé, M., Maire, A. L., Meyer, M., Rickman, E., Spalding, E. A., Asensio-Torres, R., Langlois, M., Müller, A., Baudino, J. -L., Beuzit, J. -L., Biller, B., Brandner, W., Buenzli, E., Cantalloube, F., Cheetham, A., Cudel, M., Feldt, M., Galicher, R., Janson, M., Hagelberg, J., Henning, T., Kasper, M., Keppler, M., Lagrange, A. -M., Lannier, J., LeCoroller, H., Mouillet, D., Peretti, S., Perrot, C., Salter, G., Samland, M., Schmidt, T., Sissa, E., Wildi, F. (2020), A&A, 614, 131

Luger, R., Barnes, R. (2015) Astrobiology, 15. 119

Madhusudhan N (2019) ARA&A, 57:617–663.

Madhusudhan, N., Bitsch, B., Johansen, A., Eriksson, L., (2017), MNRAS, 469, p.4102-4115.

Madhusudhan, N., Burrows, A. (2012), ApJ, 747, 25

Madhusudhan, N., Piette, A.A.A., Constantinou, S., (2021), ApJ, 918, 25

Mann AW, Gaidos E, Vanderburg A, Rizzuto AC, Ansdell M, Medina JV, Mace GN, Kraus AL and Sokal KR (2017) AJ, 153(2):64.

Marley, M.S., Sengupta, S. (2011) MNRAS, 417, 2874

Mawet D, Ruane G, Xuan W, Echeverri D, Klimovich N, Randolph M, Fucik J, Wallace JK, Wang J, Vasisht G, Dekany R, Mennesson B, Choquet E, Delorme JR and Serabyn E (2017) ApJ, 838:92.

Miles-Páez, P.A., Pallé, E., Zapatero Osorio, M.R. (2014) A&A, 562, 5

Miles-Páez, P.A., Zapatero Osorio, M.R., Pallé, E., Metchev, S. (2019) MNRAS, 484, 38

Millar-Blanchaer, M.A., Girard, J.H., Karalidi, T., Marley, M.S., van Holstein, R.G., Sengupta, S., Mawet, D., Kataria, T., Snik, F., de Boer, J., Jensen-Clem, R., Vigan, A., Hinkley, S. (2020) ApJ, 894, 42

Miller-Ricci Kempton, E. and Rauscher, E. (2012) ApJ, 751:117.

Mordasini, C., Alibert, Y., Benz, W., Klahr, H., Henning, T., (2012a) A&A, 541, 97

Mordasini, C., Alibert, Y., Georgy, C., Dittkrist, K.-M., Klahr, H., Henning, T., (2012b) A&A, 547, A112

Mordasini, C., Alibert, Y., Klahr, H., Henning, T., (2012c) A&A, 547, A111, 23

Mordasini, C., van Boekel, R., Mollière, P., Henning, Th., Benneke, B., (2016) ApJ, 832, 41

Mukherjee, S., Fortney, J.J., Jensen-Clem, R., Tan, X., Marley, M.S., Batalha, N.E. (2021) ApJ, 923, 113

Ormel CW, Liu B and Schoonenberg D (2017) A&A, 604:A1.

Pascucci I., Mulders G.D., Lopez E. (2019) ApJ, 883(1):L15.

Pecaut, M.J., Mamajek, E.E. 2013, ApJS, 208, 9.

Perryman M, Hartman J, Bakos GÁ and Lindegren L (2014) ApJ, 797(1):14.

Plavchan P, Barclay T, Gagné J, Gao P, Cale B, Matzko W, Dragomir D, Quinn S, Feliz D, Stassun K, Crossfield IJM, Berardo DA, Latham DW, Tieu B, Anglada-Escudé G, Ricker G, Vanderspek R, Seager S, Winn JN, Jenkins JM, Rinehart S, Krishnamurthy A, Dynes S, Doty J, Adams F, Afanasev DA, Beichman C, Bottom M, Bowler BP, Brinkworth C, Brown CJ, Cancino A, Ciardi DR, Clampin M, Clark JT, Collins K, Davison C, Foreman-Mackey D, Furlan E, Gaidos EJ, Geneser C, Giddens F, Gilbert E, Hall R, Hellier C, Henry T, Horner J, Howard AW, Huang C, Huber J, Kane SR, Kenworthy M, Kielkopf J, Kipping D, Klenke C, Kruse E, Latouf N, Lowrance P, Mennesson B, Mengel M, Mills SM, Morton T, Narita N, Newton E, Nishimoto A, Okumura J, Palle E, Pepper J, Quintana EV, Roberge A, Roccatagliata V, Schlieder JE, Tanner A, Teske J, Tinney CG, Vanderburg A, von Braun K, Walp B, Wang J, Wang SX, Weigand D, White R, Wittenmyer RA, Wright DJ, Youngblood A, Zhang H and Zilberman P (2020) Nature, 582(7813):497–500.

Plavchan, P., Vasisht, G., Beichman, C., Cegla, H., Dumusque, X., Wang, S.,Gao, P., Dressing, C., Bastien, F., Basu, S., Beatty, T., Bechter, A., Bechter, E., Blake, C., Bourrier, V., Cale, B., Ciardi, D., Crass, J., Crepp, J., de Kleer, K., Diddams, S., Eastman, J., Fischer, D., Gagné, J., Gaudi, S., Grier, C., Hall, R., Halverson, S., Hamze, B., Herrero Casas, E., Howard, A., Kempton, E., Latouf, N., Leifer, S., Lightsey, P., Lisse, C., Martin, E., Matzko, W., Mawet, D., Mayo, A., Newman, P., Papp, S., Pope, B., Purcell, B., Quinn, S., Ribas, I., Rosich, A., Sanchez-Maes, S., Tanner, A., Thompson, S., Vahala, K., Wang, J., Williams, P., Wise, A., Wright, J. (2020), arXiv:2006.13428

Plummer, M.K., Wang, J. (2023) ApJ, 101

Popovic, L.C., Shablovinskaya, E., Savic, D. (2022), AN, 34310089

Rackham BV, Apai D and Giampapa MS (2018) ApJ, 853(2):122.

Rajan A, Rameau J, De Rosa RJ, Marley MS, Graham JR, Macintosh B, Marois C, Morley C, Patience J, Pueyo L, Saumon D, Ward-Duong K, Ammons SM, Arriaga P, Bailey VP, Barman T, Bulger J, Burrows AS, Chilcote J, Cotten T, Czekala I, Doyon R, Duchêne G, Esposito TM, Fitzgerald MP, Follette KB, Fortney JJ, Goodsell SJ, Greenbaum AZ, Hibon P, Hung LW, Ingraham P, Johnson-Groh M, Kalas P, Konopacky Q, Lafrenière D, Larkin JE, Maire J, Marchis F, Metchev S, Millar-Blanchaer MA, Morzinski KM, Nielsen EL, Oppenheimer R, Palmer D, Patel RI, Perrin M, Poyneer L, Rantakyrö FT, Ruffio JB, Savransky D, Schnei- der AC, Sivaramakrishnan A, Song I, Soummer R, Thomas S, Vasisht G, Wallace JK, Wang JJ, Wiktorowicz S, Wolff S (2017) AJ, 154(1):10.

Reynolds, R.T., Squyres, S.W., Colburn, D.S., McKay, C.P. (1983), Icarus, 56, 246

Ridgway, R.J., Zamyatinea, M., Mayne, N.J., Manners, J., Lambert, F.H., Braam, M., Drummond, B., Hébrard, E., Palmer, P.I., Kohary, K. (2023) MNRAS, 518, 2472

Rojas Lobos, P.A., Goosmann, R.W., Hameury, J.M., Marin, F. (2020) A&A, 637, 88

Rosén, L., Kochukhov, O., Wade, G.A. (2015) ApJ, 805, 169

Rosenthal LJ, Fulton BJ, Hirsch LA, Isaacson HT, Howard AW, Dedrick CM, Sherstyuk IA, Blunt SC, Petigura EA, Knutson HA, Behmard A, Chontos A, Crepp JR, Crossfield IJM, Dalba PA, Fischer DA, Henry GW, Kane SR, Kosiarek M, Marcy GW, Rubenzahl RA, Weiss LM and Wright JT (2021), ApJS, 255, 8.

Rossi, L., Berzosa-Molina, J., Desert, J.-M., Fossati, L., Muñoz, A.G., Haswell, C., Kabath, P., Kislyakova, K., Stam, D., Vidotto, A. (2022) ExA, 54, 1187

Ruane G, Wang J, Mawet D, Jovanovic N, Delorme JR, Mennesson B and Wallace JK (2018) ApJ, 867:143.

Ruffio, J.-B., Konopacky, Q.M., Barman, T.S., Macintosh, B., Hoch, K.K.W., De Rosa, R.J., Wang, J.J., Czekala, I., Marois, C. (2021), AJ, 162, 290

Sallum, S., Follette, K.B., Eisner, J.A., Close, L.M., Hinz, P., Kratter, K., Males, J., Skemer, A., Macintosh, B., Tuthill, P., Bailey, V., Defrère, D., Morzinski, K., Rodigas, T., Spalding, E., Vax, A., Weinberger, A.J. (2015) Nature, 527, 342

Sanghavi, S., West, R., Jiang, J. (2021) ApJ, 907, 30

Savic, D., Goosmann, R., Popovic, L.C., Marin, F., Afanasiev, V.L. (2018) A&A 614, 120

Schutte, H.M., Britto, R.J., Böttcher, M., van Soelen, B., Marais, J.P., Kaur, A., Falcone, A.D., Buckley, D.A.H., Rajoelimanana, A.F., Cooper, J. (2022) ApJ, 925, 139

Seidel JV, Ehrenreich D, Pino L, Bourrier V, Lavie B, Allart R, Wyttenbach A and Lovis C (2020) A&A, 633:A86.

Sengupta, S. (2003) ApJ, 585, 155

Sengupta, S., Marley, M.S. (2016) ApJ, 824 76

Sing DK, Fortney JJ, Nikolov N, Wakeford HR, Kataria T, Evans TM, Aigrain S, Ballester GE, Burrows AS, Deming D, Désert JM, Gibson NP, Henry GW, Huitson CM, Knutson HA, Lecavelier Des Etangs A, Pont F, Showman AP, Vidal-Madjar A, Williamson MH and Wilson PA (2016) Nature, 529(7584):59–62.

Snellen IAG, Brandl BR, de Kok RJ, Brogi M, Birkby J and Schwarz H (2014) Nature, 509:63–65.

Snellen IAG, de Kok RJ, de Mooij EJW and Albrecht S (2010) Nature, 465:1049–1051.

Snellen I, de Kok R, Birkby JL, Brandl B, Brogi M, Keller C, Kenworthy M, Schwarz H and Stuik R (2015) A&A, 576:A59.

Snellen IAG, de Kok RJ, de Mooij EJW and Albrecht S (2010) Nature, 465:1049–1051.

Spiegel DS and Burrows A (2013) ApJ, 772(1):76.

Stam, D.M. (2008) A&A, 482, 989

Stevenson KB, Désert JM, Line MR, Bean JL, Fortney JJ, Showman AP, Kataria T, Kreidberg L, McCullough PR, Henry GW, Charbonneau D, Burrows A, Seager S, Madhusudhan N, Williamson MH and Homeier D (2014) Science, 346(6211):838–841.

Szulágyi, J., Garufi, A. (2021) MNRAS, 506, 73

Triaud AHMJ (2018) The Rossiter-McLaughlin Effect in Exoplanet Research, p. 2. doi:10.1007/978-3-319-55333-7_2.

Vanderburg, A., Rodriguez, J.E. (2021), ApJ, 922, 2

Vink, J.S., Harries, T.J., Drew, J.E. (2005) A&A, 430, 213

Vos, J.M., Biller, B.A., Allers, K.N., Faherty, J.K., Liu, M.C., Metchev, S., Eriksson, S., Manjavacas, E., Dupuy, T.J., Janson, M., Radigan-Hoffman, J., Crossfield, I., Bonnefoy, M., Best, W.M.J., Homeier, D., Schlieder, J.E., Brandner, W., Henning, T., Bonavita, M., Buenzli, E. (2020) AJ, 160, 38

Wade, G.A., Kudryavtsev, D., Komanyuk, I.I., Landstreet, J.D., Mathys, G. (2000) A&A, 355, 1080

Wang J, Mawet D, Ruane G, Hu R and Benneke B (2017) AJ, 153:183.

Wang JJ, Ruffio JB, Morris E, Delorme JR, Jovanovic N, Pezzato J, Echeverri D, Finnerty L, Hood C, Zanazzi JJ, Bryan ML, Bond CZ, Cetre S, Martin EC, Mawet D, Skemer A, Baker A, Xuan JW, Wallace JK, Wang J, Bartos R, Blake GA, Boden A, Buzard C, Calvin B, Chun M, Doppmann G, Dupuy TJ, Zhang J, Kempton EMR and Rauscher E (2017) ApJ, 851(2):84.

Wang, J.J., Ruffio, J.-B., Morris, E., Delorme, J.-R., Jovanovic, N., Pezzato, J., Echeverri, D., Finnerty, L., Hood, C., Zanazzi, J. J.; Bryan, M.L., Bond, C.Z., Cetre, S., Martin, E.C., Mawet, D., Skemer, A., Baker, A., Xuan, J.W., Wallace, J. K., Wang, J., Bartos, R., Blake, G.A., Boden, A., Buzard, C., Calvin, B., Chun, M., Doppmann, G., Dupuy, T.J., Duchêne, G., Feng, Y. K.,

Fitzgerald, M.P., Fortney, J., Freedman, R.S., Knutson, H., Konopacky, Q., Lilley, S., Liu, M.C., Lopez, R., Lupu, R., Marley, M.S., Meshkat, T., Miles, B., Millar-Blanchaer, M., Ragland, S., Roy, A., Ruane, G., Sappey, B., Schofield, T., Weiss, L., Wetherell, E., Wizinowich, P., Ygouf, M. (2021) AJ, 162, 148

Wagner, K., Follette, K.B., Close, L.M., Apai, D., Gibbs, A., Keppler, M., Müller, A., Henning, T., Kasper, M., Wu, Y.-L., Long, J., Males, J., Morzinski, K., McClure, M. (2018) ApJ, 863, 8

West, R.A., Yanamandra-Fisher, P.A., Korokhin, V. (2015) "Gas giant planets, Saturn's rings, and Titan", Polarimetry of Stars and Planetary Systems, 320

Williamo, T., Hackman, T., Lehtinen, J.J., Korpi-Lagg, M., Kochukhov, O. (2022) OJAp, 5, 10

Williams, J.P., Cieza, L.A. (2011), ARA&A, 49, 67

Winn J.N., Fabrycky D.C. (2015) ARA&A, 53:409–447.

Zhou, Y., Sanghi, A., Bowler, B.P., Wu, Y.-L., Close, L.M., Long, F., Ward-Duong, K., Zhu, Z., Kraus, A.L., Follette, K.B., Bae, J. (2022) ApJ, 934, 13